

# Efficient choice of coloured noise in the stochastic dynamics of open quantum systems

D. Matos<sup>1</sup>, M. A. Lane<sup>1</sup>, I. J. Ford<sup>2</sup>, and L. Kantorovich<sup>1</sup>

<sup>1</sup>*Department of Physics, King's College London,  
Strand London, WC2R 2LS, United Kingdom and*

<sup>2</sup>*Department of Physics and Astronomy, University College London,  
Gower Street, London, WC1E 6BT, United Kingdom*

The Stochastic Liouville-von Neumann (SLN) equation describes the dynamics of an open quantum system reduced density matrix coupled to a non-Markovian harmonic environment. The interaction with the environment is represented by complex coloured noises which drive the system, and whose correlation functions are set by the properties of the environment. We present a number of schemes capable of generating coloured noises of this kind that are built on a noise amplitude reduction procedure [Imai *et al*, Chem. Phys. 446, 134 (2015)], including two analytically optimised schemes. In doing so, we pay close attention to the properties of the correlation functions in Fourier space, which we derive in full. For some schemes the method of Wiener filtering for deconvolutions leads to the realisation that weakening causality in one of the noise correlation functions improves numerical convergence considerably, allowing us to introduce a well controlled method for doing so. We compare the ability of these schemes, along with an alternative optimised scheme [Schmitz and Stockburger, Eur. Phys. J.: Spec. Top. **227**, 1929 (2019)], to reduce the growth in the mean and variance of the trace of the reduced density matrix, and their ability to extend the region in which the dynamics is stable and well converged for a range of temperatures. By numerically optimising an additional noise scaling freedom, we identify the scheme which performs best for the parameters used, improving convergence by orders of magnitude and increasing the time accessible by simulation.

## I. INTRODUCTION

In open quantum systems, interactions between the system of interest and its environment drive behaviours such as dissipation and decoherence which are not found in isolation. These play a strong role in quantum computing<sup>1</sup> where the ability of the open system to stay in a superposition of states is desirable, and also in quantum thermodynamics<sup>2</sup>. Unfortunately, the very large number of environmental degrees of freedom makes the treatment of both the system and environment analytically and numerically challenging, especially when there is strong coupling between them. For this reason, existing methods tend to begin by taking the partial trace of the full density matrix over the environment variables to obtain the reduced density matrix of the system of interest. In particular, this is done in the well-known Feynman-Vernon influence functional formalism where the response of a bath coupled linearly to the open system is expressed as a path integral over an infinite number of displaced harmonic oscillators<sup>3</sup>. Techniques which build on this method include hierarchical equations of motion (HEOM)<sup>4-6</sup>, hybrid stochastic HEOM<sup>7,8</sup>, hierarchy of pure states<sup>9</sup>, stochastic Schrödinger equations<sup>10</sup>, quadiabatic path integrals<sup>11</sup>, Stochastic Liouville-von Neumann equations (SLNs)<sup>12-15</sup>, and the Extended SLN (ESLN) equations method, which accounts for initial thermalisation by the inclusion of an additional stochastic differential equation (SDE) in imaginary time with imaginary time noises<sup>16-18</sup>. Importantly, none of these methods make the Markov assumption, where the environment correlation times are taken to be negligibly short compared to the characteristic timescales of the open system. The Markov assumption has the physical interpretation that any information dissipated from the system to the environment will never be returned, i.e. the system-environment coupling is memoryless. Instead, the environment is allowed to be fully non-Markovian, introducing a source of memory to the system.

The SLN and ESLN methods, amongst others, are based on solving SDEs with complex correlated (coloured) Gaussian noises. Beginning with the seminal work of Grabert, Schramm and Ingold<sup>19</sup>, these methods evolve stochastic reduced density matrices via SDEs, driven by the aforementioned noises, with the physical density matrix being recovered by stochastic averaging over all realisations of these noises. The advantage of these methods is that they are exact, non-perturbative, and are in principle applicable to any temperature, system-environment coupling strength, and any form of the spectral density. In addition, with the recent development of the ESLN, the system and its environment can be thermalised via the application of an initial evolution in imaginary time, rather than being initialised in a partitioned state<sup>12-15</sup>. The current work focuses on the properties of the noises and their generation rather than on thermalisation or the properties of specific physical dynamics, so we shall limit ourselves to the SLN rather than the ESLN for simplicity. It is important to note that these methods do not constitute an *ad hoc* representation of the system behaviour where the noises might have been introduced artificially to model the environment. Instead, they have been derived rigorously from an appropriate consideration of the whole system, consisting of both the open system and its environment, by means of elimination of the environment using the path-integral method and a Hubbard-Stratonovich transformation.

To simulate these SDEs, particular care must be taken when generating the complex coloured noises, as the choice of a generation scheme can significantly alter the statistical properties of the noises and thus the system dynamics. A poor choice is characterised by a catastrophic loss of trace preservation for the reduced density matrix, which requires an exponentially large sample for convergence of the average. Making this choice is not trivial since the correlation functions must be satisfied with sensible decisions being made wherever there is freedom to do so, especially for stronger coupling when the magnitude of the noises is already large. In fact, one of the main conclusions of this work is that generating noises which satisfy the desired correlation functions is not enough to guarantee convergence or that the results be physical, despite the correlation functions being the only formal requirements of the theory on the noises.

In our previous work<sup>18</sup>, one particular noise generation scheme was used which produced well converged results as a verification of the ESLN method, but here we generalise our procedure and explore a number of possible noise generation schemes which all create the desired correlation functions but produce results of different convergence for the open system dynamics. We also optimise the scheme to minimise the (erroneous) exponential growth of the trace, something which has only recently been studied in any detail<sup>18,20,21</sup>, though with some inconsistencies in<sup>20</sup> which we correct, and compare our optimised scheme with a recently proposed alternative, obtained independently via a different method and optimised subject to different constraints<sup>21</sup>. By examining the properties of the Fourier transforms of the desired correlations, the properties of the different noises, and their effect on the system dynamics, we arrive at a number of conclusions about noise generation for SLN methods, where and why issues arise, and how to maximise the possible duration (run time) of simulations before the stochastic nature of the dynamics inevitably leads to numerical blow up and statistical uncertainty.

For this purpose, we will use the spin-boson model as it is a relatively simple model consisting of a two-level spin system surrounded by bosonic degrees of freedom that describe the environment. This can naturally be applied to qubits coupled to an environment<sup>22-26</sup>, electronic energy transfer in biological systems<sup>20</sup>, Josephson junctions<sup>27-29</sup>, cold atoms<sup>30,31</sup> and solid-state artificial atoms<sup>32</sup>. The spin-boson model has already been considered previously by us in the context of the ESLN<sup>18</sup>.

Comparison with other methods mentioned in the Introduction is not within the scope of this paper, as it will be focusing only on the details of the noise generation within the SLN equation formalism. So, the purpose of the present paper is fourfold: (1) develop a general scheme for noise generation for the SLN equation and propose a number of possible choices for the scheme, including a fully optimised choice, (2) demonstrate that these choices significantly alter the properties of the noises with appropriate use of deconvolution methods<sup>33,34</sup> where necessary, (3) examine in detail how different choices affect the convergence properties of the results and the accessible run time of simulation before blow up, comparing with other optimisation schemes where possible<sup>20,21</sup>, and (4) explain in detail why particular choices fail, referring to the properties of the correlation functions themselves where necessary. More concretely, in Sec. II we briefly review the SLN formalism and the spin-boson model, before introducing in Sec. III our specific framework for noise generation and the possible choices we have identified. Finally in Sec. IV we present the results of the various noise generation schemes.

## II. THEORY

### A. Stochastic Liouville-von Neumann equations

Following the influence functional formalism of Feynman and Vernon<sup>3</sup>, we consider the standard setup of an open quantum system with coordinates  $q$  and Hamiltonian  $H_q$  (that may describe either an electronic or bosonic subsystem, or both) coupled to an environmental heat bath of harmonic oscillators  $i$  with masses  $m_i$ , governed by a potential energy that is quadratic in the oscillator displacement coordinates  $\xi_i$ . The coupling between the open system and its environment is linear in the environment coordinates but fully general in  $q$ , taking the form  $-\xi_i f_i(q)$  for the given coordinate  $\xi_i$ , with the  $f_i(q)$  being arbitrary functions of  $q$ . The full system Hamiltonian is thus

$$H_{\text{tot}}(q, \{\xi_i\}, t) = H_q(q, t) + \sum_i \frac{p_i^2}{2m_i} + \frac{1}{2} \sum_{ij} \Lambda_{ij} \xi_i \xi_j - \sum_i \xi_i f_i(q), \quad (1)$$

where  $p_i$  are momentum coordinates canonical to  $\xi_i$ , and  $\Lambda_{ij}$  is the force constant matrix of the bath. This is a more general form of the Caldeira-Leggett Hamiltonian<sup>35</sup> since the environment coupling is a general function of  $q$  rather than being strictly bilinear.

In the SLN method the open system and environment density matrices are initialised in a partitioned state where the full density matrix  $\rho_0 = \rho_{\text{tot}}(t_0)$  is the tensor product of the open system density matrix  $\rho_q(t_0)$  and that of its environment  $\rho_\xi(t_0)$  at some initial time  $t_0$ ,

$$\rho_0 = \rho_q(t_0) \otimes \rho_\xi(t_0). \quad (2)$$

In principle, the open system and its environment can be initialised in the canonical equilibrium state using the ESLN formalism<sup>16,18</sup>, with the system and environment in thermal contact such that they are fully thermalised. However, here we shall limit ourselves to the partitioned initial state [Eq. (2)] and the SLN method.

Tracing over the environment variables<sup>15,19</sup>, it is possible to obtain the Stochastic Liouville-von Neumann (SLN) equation, an SDE which describes the evolution of a stochastic reduced density matrix for the system driven by complex coloured noises, where the physical reduced density matrix is obtained by taking the average over a sample of many realisations of the dynamics. This SLN takes the form

$$i\hbar \frac{d\rho(t)}{dt} = [H_q(t), \rho(t)] - \eta(t) [f(q), \rho(t)] - \frac{\hbar}{2} \nu(t) \{f(q), \rho(t)\}, \quad (3)$$

where  $\rho(t)$  represents the stochastic reduced density matrix and the square (curly) brackets represent standard (anti-)commutators, with the physical reduced density matrix given by  $\rho^{\text{ph}}(t) = \langle \rho(t) \rangle$ . Here,  $\eta(t)$  and  $\nu(t)$  are the aforementioned complex coloured noises, angle brackets  $\langle \dots \rangle$  represent an average over the noises,  $H_q(t)$  is the open system Hamiltonian mentioned previously (which may depend explicitly on time), and  $f(q)$  is the (universal) function which couples the system to the environmental oscillators, assumed to be time independent.

The noises all have zero mean and are otherwise defined by their correlation functions

$$\langle \eta(t)\eta(t') \rangle = \hbar \int_0^\infty \frac{d\omega}{\pi} J(\omega) \coth\left(\frac{1}{2}\beta\hbar\omega\right) \cos(\omega(t-t')) \equiv K_{\eta\eta}(t-t'), \quad (4)$$

$$\langle \eta(t)\nu(t') \rangle = -2i\Theta(t-t') \int_0^\infty \frac{d\omega}{\pi} J(\omega) \sin(\omega(t-t')) \equiv K_{\eta\nu}(t-t') = iR(t-t'), \quad (5)$$

$$\langle \nu(t)\nu(t') \rangle = 0, \quad \forall t, t', \quad (6)$$

where  $J(\omega)$  is the spectral density of the environment and  $\beta = 1/k_B T$  where  $T$  is the temperature of the environment. From now on we set  $\hbar = 1$ . In this study we take  $J(\omega)$  to be of the Drude form

$$J(\omega) = \omega \left[ 1 + \left( \frac{\omega}{\omega_c} \right)^2 \right]^{-2}, \quad (7)$$

where the cut off frequency  $\omega_c$  controls the decaying character of  $J(\omega)$  at large  $\omega$ , and there is a hard cutoff such that  $J(\omega > \omega_c) = 0$ . To be explicit, the Drude form of the spectral density is used prior to a hard cutoff  $\omega_c$  that specifies the maximum phonon frequency of the bath above which there is no contribution associated with higher frequencies.

## B. Spin-Boson Model

Thus far, the system Hamiltonian  $H_q$  has been kept fully general, as has the form of the system-environment coupling,  $f(q)$ . We will adopt the spin-boson Hamiltonian for our system of interest which, in a basis of a generic two-state system, is

$$H_q(t) = \frac{1}{2}\Delta(t)\sigma_x + \frac{1}{2}\epsilon(t)\sigma_z = \frac{1}{2}\Delta(t)(|0\rangle\langle 1| + |1\rangle\langle 0|) + \frac{1}{2}\epsilon(t)(|0\rangle\langle 0| - |1\rangle\langle 1|). \quad (8)$$

Here,  $\sigma_{x,y,z}$  are the standard Pauli spin matrices with  $\sigma_x$  flipping the spin from one state to the other with tunnelling strength  $\Delta(t)$  and  $\sigma_z$  biasing the energy of states with magnitude  $\epsilon(t)$ . The system-bath coupling (previously  $f(q)$  in Eq. (3)) is  $\alpha\sigma_z$ , where  $\alpha$  is the coupling strength between the open system and the environmental oscillators. Equation (3) then becomes

$$i \frac{d\boldsymbol{\rho}(t)}{dt} = [H(t), \boldsymbol{\rho}(t)] - \alpha\eta(t) [\sigma_z, \boldsymbol{\rho}(t)] - \frac{1}{2}\alpha\nu(t) \{\sigma_z, \boldsymbol{\rho}(t)\}. \quad (9)$$

Finally, for the spin-boson Hamiltonian it is straightforward to derive coupled SDEs for the  $x$ -,  $y$ - and  $z$ -spins and  $\text{Tr}\boldsymbol{\rho}(t)$  directly,

$$\frac{d\sigma_x(t)}{dt} = -[\epsilon(t) - 2\alpha\eta(t)]\sigma_y(t) \quad (10)$$

$$\frac{d\sigma_y(t)}{dt} = -\Delta(t)\sigma_z(t) + [\epsilon(t) - 2\alpha\eta(t)]\sigma_x(t) \quad (11)$$

$$\frac{d\sigma_z(t)}{dt} = \Delta(t)\sigma_y(t) + i\alpha\nu(t)\text{Tr}\boldsymbol{\rho}(t) \quad (12)$$

$$\frac{d\text{Tr}\boldsymbol{\rho}(t)}{dt} = i\alpha\nu(t)\sigma_z(t). \quad (13)$$

To be clear, these are expectation values of spins  $\sigma_{x,y,z}(t) = \text{Tr}(\sigma_{x,y,z}\boldsymbol{\rho}(t))$  obtained from a single realisation of the stochastic reduced density matrix. The physical expectation values would then be obtained by the average over many such realisations,  $\langle \sigma_{x,y,z}(t) \rangle$ .

### III. NOISE GENERATION SCHEMES

The correlation functions given by Eqs. (4)-(6) act as constraints on the noise generated, but do not uniquely define them, leaving some freedom to specify the generation procedure.

For the purpose of considering different representations of the noises, we adopt the most general form of the linear filtering ansatz<sup>36</sup>,

$$\eta(t) = \int_{-\infty}^{\infty} dt' \sum_j F_j f_j(t-t') x_j(t') \quad (14)$$

$$\nu(t) = \int_{-\infty}^{\infty} dt' \sum_j G_j g_j(t-t') x_j(t'), \quad (15)$$

where the  $\{f_j\}$  and  $\{g_j\}$  are real functions of time (henceforth referred to as filters) which must be chosen such that the correlation functions of Eqs. (4)-(6) are satisfied.  $F_j$  and  $G_j$  are either 1 or the imaginary unit  $i$  and are also chosen to be consistent with the correlation functions, and the  $\{x_j\}$  are real valued white Gaussian uncorrelated noises.

#### A. Orthogonal Decomposition

The form used above has the benefit that it is possible, if desired, to decompose each noise into orthogonal components that are correlated with only one other component<sup>17,18</sup>. This orthogonality can, e.g., be achieved by expressing the noises as

$$\eta(t) = \int_{-\infty}^{\infty} dt' f_1(t-t') x_1(t') + \int_{-\infty}^{\infty} dt' f_2(t-t') [x_2(t') + i x_3(t')] \quad (16)$$

$$\nu(t) = \int_{-\infty}^{\infty} dt' g_1(t-t') [i x_1(t') + x_4(t')] + \int_{-\infty}^{\infty} dt' g_2(t-t') [x_3(t') + i x_2(t')], \quad (17)$$

While it is possible to add an arbitrary number of terms of the appropriate form containing pairs of noises as is done here, we consider no more than one such term in the expansion of  $\eta(t)$  and up to two in  $\nu(t)$ , since this restricts the number of necessary white noises to the minimum possible number. We emphasise that while this does represent a loss of generality compared to Eqs. (14) and (15), there are three benefits. First, autocorrelative and cross-correlative components of the noise can be immediately identified by their structure, with, e.g., the first term of Eq. (16) being autocorrelative while the second term is cross-correlative. Second, the noise can be decomposed into orthogonal components which are co-correlated with only one other component. For example, the term involving  $f_2$  is correlated only with the term involving  $g_2$  and no other terms. And third, forming complex noise from pairs of real noises ensures that their autocorrelation vanishes by construction. This is especially useful for the  $\nu$  noise which has zero self-correlation.

The choice of filters  $f_1$ ,  $f_2$ ,  $g_1$  and  $g_2$  is then made by relating the expectation values of the noises to the appropriate correlation functions, Eqs. (4)-(6), and taking Fourier transforms (indicated by a tilde). In particular,

$$\tilde{K}_{\eta\eta}(\omega) = \tilde{f}_1(\omega) \tilde{f}_1(-\omega). \quad (18)$$

Note that  $\tilde{f}^*(\omega) = \tilde{f}(-\omega)$  for any real function  $f(t)$ . Since  $K_{\eta\eta}(t)$  is real and even, its Fourier transform is also real and even, so  $\tilde{K}_{\eta\eta}(\omega) = \tilde{K}_{\eta\eta}(-\omega)$ , and thus it is convenient to choose  $\tilde{f}_1(\omega)$  to be real, hence

$$\tilde{K}_{\eta\eta}(\omega) = \tilde{f}_1(\omega)^2 \quad \Rightarrow \quad \tilde{f}_1(\omega) = \sqrt{\tilde{K}_{\eta\eta}(\omega)}, \quad (19)$$

thus specifying the autocorrelative filter,  $\tilde{f}_1(\omega)$ .

The correlation between  $\eta$  and  $\nu$ ,  $K_{\eta\nu}(t)$  of Eq. (20), requires that the following constraint in Fourier space be

satisfied:

$$\tilde{f}_1(\omega)\tilde{g}_1(-\omega) + 2\tilde{f}_2(\omega)\tilde{g}_2(-\omega) = \tilde{R}(\omega), \quad (20)$$

where  $R(t) = -iK_{\eta\nu}(t)$  [Eq. (5)]; note that  $R(t)$  is a real function. Derivations of the Fourier transforms  $\tilde{K}_{\eta\eta}(\omega)$  and  $\tilde{K}_{\eta\nu}(\omega)$  and their properties are provided in Appendices A 1 and A 2. The three filters  $\tilde{g}_1(\omega)$ ,  $\tilde{f}_1(\omega)$  and  $\tilde{f}_2(\omega)$  are determined by only a single condition [Eq. (20)], and hence their full specification is subject to different possible choices, some of which we now discuss.

### 1. Delta Scheme

Choosing  $g_1$  to be zero and  $g_2(t)$  to be a  $\delta$  function, gives

$$f_2(t) = -\frac{i}{2}K_{\eta\nu}(t) \quad (21)$$

$$g_2(t) = \delta(t). \quad (22)$$

This choice can be reversed by switching the  $\delta$  function around. For obvious reasons, we refer to this as the *delta* choice; it was made in previous work<sup>17</sup>.

### 2. Constrained choice

Taking the constraint Eq. (20) and setting  $\tilde{f}_2$  and  $\tilde{g}_2$  to be zero, this becomes a decomposition with  $\tilde{f}_1$  given by Eq. (19) and  $\tilde{g}_1$  given by

$$\tilde{g}_1(\omega) = \frac{\tilde{R}(-\omega)}{\sqrt{\tilde{K}_{\eta\eta}(\omega)}}. \quad (23)$$

We refer to this as the *constrained* choice, since the two filters  $\tilde{f}_1(\omega)$  and  $\tilde{g}_1(\omega)$  are fully constrained (defined) with no flexibility.

### 3. Like Scheme

In a similar fashion,  $\tilde{g}_1(\omega)$  can be set to zero instead of  $\tilde{f}_2(\omega)$  and  $\tilde{g}_2(\omega)$ , in which case Eq. (20) becomes

$$\tilde{f}_2(\omega)\tilde{g}_2(-\omega) = \frac{1}{2}\tilde{R}(\omega). \quad (24)$$

A possible choice for  $\tilde{f}_2(\omega)$  and  $\tilde{g}_2(\omega)$  is to require that  $\tilde{f}_2(\omega) = \tilde{g}_2(-\omega)$  such that

$$\tilde{f}_2(\omega) = \sqrt{\frac{1}{2}\tilde{R}(\omega)} = \sqrt{-\frac{i}{2}\tilde{K}_{\eta\nu}(\omega)}, \quad (25)$$

with  $\tilde{g}_2(\omega)$  simply given by sending  $\omega \rightarrow -\omega$  on the right hand side. For obvious reasons, we refer to this choice as the *like* choice: it has been used by us previously<sup>18</sup>.

### 4. Reduced Scheme

Any combination of the *like* and *constrained* choices will also be allowed, since they would satisfy the general definitions of the noises Eqs. (16) and (17). We introduce a set of filters  $\tilde{f}_1$ ,  $\tilde{f}_2$ ,  $\tilde{g}_1$  and  $\tilde{g}_2$  which utilise both of the

above choices via the introduction of an auxiliary mixing function  $\tilde{A}(\omega)$ ,

$$\tilde{f}_1(\omega) = \sqrt{\tilde{K}_{\eta\eta}(\omega)} \quad (26)$$

$$\tilde{f}_2(\omega) = \sqrt{\frac{1}{2}\tilde{A}(\omega)\tilde{R}(\omega)} \quad (27)$$

$$\tilde{g}_1(\omega) = \frac{\tilde{R}(-\omega)}{\sqrt{\tilde{K}_{\eta\eta}(\omega)}} [1 - \tilde{A}(-\omega)] \quad (28)$$

$$\tilde{g}_2(\omega) = \sqrt{\frac{1}{2}\tilde{A}(-\omega)\tilde{R}(-\omega)}. \quad (29)$$

Here, the mixing function  $\tilde{A}(\omega)$  controls which of the two choices (*like* and/or *constrained*) is being used at each value of  $\omega$ , and it is easy to verify that these filters satisfy Eq. (20). A similar expression was recently presented<sup>20</sup>, though due to incorrect definitions of the filters it was neither general nor correct, as the properties of the Fourier transforms (see Appendix A) were not satisfied in any case except for the autocorrelative component of  $\eta$  which is already fully determined. The special cases of  $\tilde{A}(\omega) = 0$  and  $\tilde{A}(\omega) = 1$  correspond to the *constrained* and *like* choices, respectively.

By examination of the evolution of  $\text{Tr}(\rho(t))$  [Eq. (13)], it is clear that the non-Hermitian (trace non-preserving) dynamics of the stochastic density matrix is driven solely by  $\nu$ . The spread of values of the trace will grow with time, just as the variance of the displacement of a Brownian walker grows with time, and this spreading requires an ever larger ensemble of realisations for the average trace to remain close to unity at late times. We thus try to choose the mixing function  $\tilde{A}(\omega) = \{0, 1\}$  to reduce the average amplitude of  $\nu(t)$ , noting that

$$\langle |\nu(t)|^2 \rangle = \int \frac{d\omega}{2\pi} \left\{ 2 \frac{|\tilde{R}(-\omega)|^2}{\tilde{K}_{\eta\eta}(\omega)} |1 - \tilde{A}(-\omega)|^2 + |\tilde{R}(-\omega)| |\tilde{A}(-\omega)| \right\}. \quad (30)$$

We choose  $\tilde{A}(\omega) = 0$  when the first term in the integrand is smaller than the second term; otherwise  $\tilde{A}(\omega)$  should be 1, that is (cf. Ref.<sup>20</sup>)

$$\tilde{A}(\omega) = \begin{cases} 0, & \text{when } |\tilde{R}(-\omega)|^2 / \tilde{K}_{\eta\eta}(\omega) \leq |\tilde{R}(-\omega)| \\ 1, & \text{otherwise.} \end{cases} \quad (31)$$

This choice, which can be done individually for every value of  $\omega$ , should then significantly reduce the average magnitude of  $\nu(t)$ , diminishing the impact of the non-Hermitian dynamics and improving the convergence of the ensemble average. Thus we refer to this as the *reduced* choice.

## 5. Optimised Scheme

This naturally leads us to choosing the optimal mixing function  $\tilde{A}(\omega)$  which truly minimises the average magnitude of  $\nu$ ; this is the  $\nu$ -*optimised* choice. Starting with Eq. (20), it can be shown that the mixing function must be real and even (see Appendix B). By setting the derivative of Eq. (30) with respect to  $\tilde{A}(\omega)$  equal to zero, we find the  $\nu$ -optimised mixing function to be

$$\tilde{A}(\omega) = 1 - \frac{\tilde{K}_{\eta\eta}(\omega)}{4|\tilde{R}(\omega)|}. \quad (32)$$

Substituting this  $\tilde{A}(\omega)$  into Eqs. (27) and (29) gives the corresponding filters as

$$\tilde{f}_2(\omega) = \sqrt{\frac{\tilde{R}(\omega)}{2} \left( 1 - \zeta \frac{\tilde{K}_{\eta\eta}(\omega)}{|\tilde{R}(\omega)|} \right)} \quad (33)$$

$$\tilde{g}_1(\omega) = \zeta \frac{\tilde{R}(-\omega)}{|\tilde{R}(\omega)|} \sqrt{\tilde{K}_{\eta\eta}(\omega)} \quad (34)$$

$$\tilde{g}_2(\omega) = \sqrt{\frac{\tilde{R}(-\omega)}{2} \left( 1 - \zeta \frac{\tilde{K}_{\eta\eta}(\omega)}{|\tilde{R}(\omega)|} \right)} \quad (35)$$

with  $\tilde{f}_1(\omega) = \sqrt{\tilde{K}_{\eta\eta}(\omega)}$  as before, and  $\zeta = 1/4$ .

An alternative approach would be to minimise  $\langle |\eta(t)|^2 \rangle + \langle |\nu(t)|^2 \rangle$  rather than just the average magnitude of  $\nu$ , by considering

$$\langle |\eta(t)|^2 \rangle + \langle |\nu(t)|^2 \rangle = \int \frac{d\omega}{2\pi} \left\{ \tilde{K}_{\eta\eta}(\omega) + |\tilde{R}(\omega)| \left( |\tilde{A}(\omega)| + |\tilde{A}(-\omega)| \right) + 2 \frac{|\tilde{R}(\omega)|^2}{\tilde{K}_{\eta\eta}(\omega)} |1 - \tilde{A}(-\omega)|^2 \right\}$$

for which the minimising mixing function is

$$\tilde{A}(\omega) = 1 - \frac{\tilde{K}_{\eta\eta}(\omega)}{2|\tilde{R}(\omega)|},$$

with its own  $\tilde{f}_2$ ,  $\tilde{g}_1$  and  $\tilde{g}_2$ , which are defined by the same Eqs. (33)-(35), but with  $\zeta = 1/2$ . We refer to this as the  $\eta\nu$ -*optimised* scheme.

The derivations of the minimising mixing function for both optimised choices are presented in Appendix B.

It is important to stress that minimising the combined magnitude  $\langle |\eta(t)|^2 \rangle + \langle |\nu(t)|^2 \rangle$  will not necessarily minimise the variance of the trace, nor the rate of its exponential growth. As far as we are aware it is not possible to analytically minimise the growth of the trace directly, so we are forced to approach any optimisation via an ansatz, in this case by introducing the mixing function and making use of the freedom in its definition. While the optimal mixing functions derived here affect the properties of the noises as intended, they do not guarantee that the behaviour of the trace will be modified in the desired way for all parameters or over all timescales. This approach should be thought of as an indirect optimisation of the properties of the dynamics.

## 6. Dynamical Rescaling

It is possible to go one step further by introducing a dynamical rescaling of the cross-correlative filters  $\tilde{f}_2$  and  $\tilde{g}_2$ , as was done for the *like* scheme in previous work<sup>18</sup>. This type of scaling was first introduced for autocorrelative coloured noises in Ref.<sup>37</sup>, and expanded to cross-correlative noises in Ref.<sup>18</sup>. Since dividing  $\tilde{f}_2(\omega)$  by an arbitrary  $\omega$ -dependent factor  $\tilde{\chi}(\omega)$  and multiplying  $\tilde{g}_2(\omega)$  by the same factor will leave the correlation  $K_{\eta\nu}$  between  $\eta$  and  $\nu$  unchanged, we can choose this factor optimally. However attempting to minimise  $\langle |\eta(t)|^2 \rangle + \langle |\nu(t)|^2 \rangle$  with respect to  $\tilde{\chi}(\omega)$  in Fourier space for each  $\omega$  gives the result that  $\tilde{\chi}(\omega) = \pm 1, \pm i$ , which is trivial.

As stated above, while this is the  $\tilde{\chi}(\omega)$  which minimises the combined magnitude of the noises, it is more desirable to minimise the growth of the trace directly. For this reason we consider a similar scaling in the time domain, instead dividing  $f_2(t)$  by a scaling factor and multiplying  $g_2(t)$  by that same number, even though the scaling freedom is most apparent in Fourier space. We can then choose the scaling factor to minimise the rate of spreading of  $|\text{Tr}\rho(t)|$ . We do this by sampling the final value of the trace for a range of scaling factors and minimising the standard error in the mean trace. Note that where the optimisation of the mixing function  $\tilde{A}$  was analytical, choosing this optimal scaling is a numerical procedure.

It is convenient to implement this scaling via the ratio between the noises generated using  $f_2$  and  $g_2$  before any scaling is applied, denoted here as  $\eta_0$  and  $\nu_0$ , respectively. The scaled noises are then obtained from the unscaled

noises as  $\eta^{new} = \lambda_{\nu\eta}\eta_0$  and  $\nu^{new} = \nu_0/\lambda_{\nu\eta}$ , where

$$\lambda_{\nu\eta} = \sqrt{\lambda} \sqrt{\frac{\sum_n |\nu_0(t_n)|}{\sum_n |\eta_0(t_n)|}}, \quad (36)$$

and  $\lambda$  is a parameter (to be determined) representing the desired ratio between  $\nu^{new}$  and  $\eta^{new}$ . Here, the sums are over a single realisation of the noises in time, adding the value of the noise at each discrete time,  $t_n$ .

### B. Convex Optimised Scheme

It is also possible to optimise the noise generation scheme in a different manner using the general form of the noises (14) and (15), without explicitly introducing a mixing function<sup>21</sup>. Instead of minimising the average of the square magnitude of  $\nu$  or the sum of square magnitudes of  $\nu$  and  $\eta$ , the sum of the imaginary parts of  $\eta$  and  $\nu$  can be minimised, subject to the correlations, by the method of convex optimisation. We can reproduce the analytical expression obtained in Ref.<sup>21</sup> for the correlations of the real and imaginary components of the noises  $\eta$  and  $\nu$  using the following forms,

$$\eta(t) = \int_{-\infty}^{\infty} dt' f_1(t-t') x_1(t') + i \int_{-\infty}^{\infty} dt' f_2(t-t') x_2(t') \quad (37)$$

$$\nu(t) = \int_{-\infty}^{\infty} dt' g_1(t-t') [x_1(t') + ix_2(t')]. \quad (38)$$

The filters in Fourier space can be written as

$$\tilde{f}_1(\omega) = \frac{1 - \tilde{C}(\omega)}{\sqrt{1 - 2\tilde{C}(\omega)}} \sqrt{\tilde{K}_{\eta\eta}(\omega)} \quad (39)$$

$$\tilde{f}_2(\omega) = \frac{\tilde{C}(\omega)}{\sqrt{1 - 2\tilde{C}(\omega)}} \sqrt{\tilde{K}_{\eta\eta}(\omega)} \quad (40)$$

$$\tilde{g}_1(\omega) = \sqrt{1 - 2\tilde{C}(\omega)} \frac{\tilde{R}(-\omega)}{\sqrt{\tilde{K}_{\eta\eta}(\omega)}}, \quad (41)$$

where

$$\tilde{C}(\omega) = \frac{1}{2} \left[ 1 - \left( \frac{4 |\tilde{R}(\omega)|^2}{\tilde{K}_{\eta\eta}(\omega)^2} + 1 \right)^{-1/2} \right]. \quad (42)$$

### C. Deconvolution for Reduced and Constrained Schemes

Division in Fourier space can introduce troublesome amplification for frequencies near which the denominator is close to zero<sup>34,38</sup> (see, for example, Eq. (23).) The  $\tilde{C}(\omega)$  function in the convex optimised scheme removes explicit divisions where this would occur and can be implemented as it stands, as it involves only division by  $4 |\tilde{R}(\omega)|^2 + \tilde{K}_{\eta\eta}(\omega)^2$ . The same applies to the  $\nu$ -optimised and  $\eta\nu$ -optimised schemes where the filters remain finite since  $\tilde{R}/|\tilde{R}|$  has real and imaginary parts which are bounded by  $\pm 1$ . Thus the constrained and reduced

schemes are the only schemes which include explicit division by a filter in Fourier space, in this case by  $\sqrt{\tilde{K}_{\eta\eta}(\omega)}$  in Eqs. (23) and (28), so they require additional care.

This issue of frequency amplification around the zeros of  $\sqrt{\tilde{K}_{\eta\eta}(\omega)}$  can be eased by deconvolution methods. A deconvolution is the inverse operation to a convolution which can be naively interpreted as division in Fourier space. In practice, the process is more complex. Even for two deterministic functions, there is always an issue of division close to zero, or of rounding errors which can cause numerical instabilities in the deconvolved signal after taking the inverse Fourier transform<sup>33,34</sup>. In particular, these instabilities can depend on properties of the signal such as its length  $t_{max}$  and spacing  $\Delta t$ , since these affect the sensitivity of the Fourier transform to small numbers.

We adopt the deconvolution method of Wiener filtering<sup>39</sup> which minimises the mean square error between some desired quantity  $q(t)$  to be determined and its estimate  $\hat{q}(t)$ . Considering the signal associated with  $q(t)$  to be

$$y(t) = \int dt' h(t-t') q(t') + \xi(t), \quad (43)$$

where  $h(t)$  is the known response function of  $q(t)$  and  $\xi(t)$  is some unknown noise, the estimate of the signal in the time domain is

$$\hat{q}(t) = \int dt' w(t-t') y(t'), \quad (44)$$

where we have introduced some ‘‘inverse’’ to the response function,  $w(t)$ . In Fourier space this becomes

$$\tilde{q}(\omega) = \tilde{W}(\omega) \tilde{Y}(\omega), \quad (45)$$

with

$$\tilde{W}(\omega) = \frac{\tilde{H}^*(\omega)}{|\tilde{H}(\omega)|^2 + \frac{1}{\text{SNR}}}. \quad (46)$$

being the Fourier transform of the inverse response function  $w(t)$ . Here  $\tilde{H}(\omega)$  and  $\tilde{Y}(\omega)$  are the Fourier transforms of  $h(t)$  and  $y(t)$ , respectively. This  $\tilde{W}(\omega)$  is known as the Wiener filter and is used as an estimate of  $\tilde{H}(\omega)$  with the problematic frequency amplification removed. It arises directly from minimising the mean square error  $\mathbb{E}|\hat{q}(t) - q(t)|^2$ <sup>38,40</sup>. Finally, SNR is the signal to noise ratio, or, more concretely, it is the ratio between the mean power spectral densities of the signal and the noise. Typically for the Wiener filter, the SNR needs to be estimated in some way, especially when the form of the noise  $\xi(t)$  is not exactly known<sup>38,40</sup>, and is usually chosen to be a constant value such that the signal is guaranteed to be larger than the noise.

Adopting this method, the division by  $\sqrt{\tilde{K}_{\eta\eta}}$  in the constrained and reduced schemes should be replaced with multiplication by the corresponding Wiener filter,

$$\frac{1}{\sqrt{\tilde{K}_{\eta\eta}(\omega)}} \rightarrow \frac{\sqrt{\tilde{K}_{\eta\eta}(\omega)}}{\tilde{K}_{\eta\eta}(\omega) + \gamma \max_{\omega} \left| \sqrt{\tilde{K}_{\eta\eta}(\omega)} \right|}, \quad (47)$$

with a signal to noise ratio  $\text{SNR} = \left( \gamma \max_{\omega} \left| \sqrt{\tilde{K}_{\eta\eta}(\omega)} \right| \right)^{-1}$  where  $\gamma$  is a small parameter. This allows the correction term to vary depending on the simulation time  $t_{max}$ , and to stabilise the division while still remaining small. Note that this is something of a numerical fix; it will modify the correlation function  $\langle \eta(t) \nu(t') \rangle$  so that it no longer matches the desired correlation  $K_{\eta\nu}(t-t')$  [Eq. (5)] exactly, though the introduction of the small parameter  $\gamma$  allows us to control the size of this deviation.

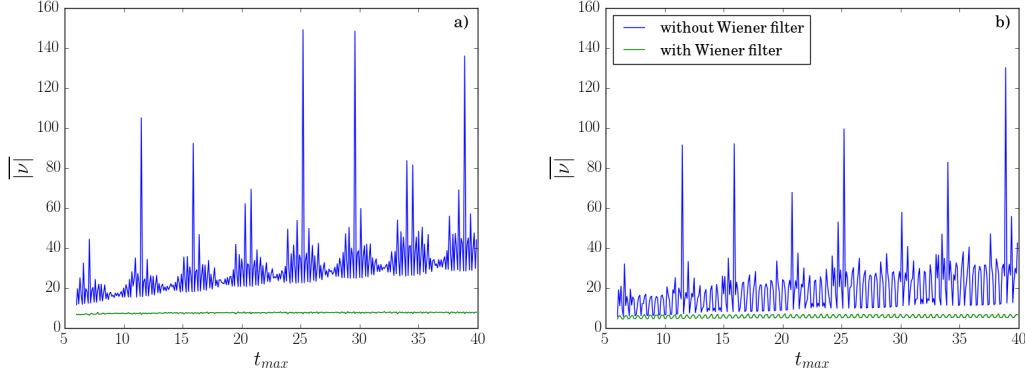


FIG. 1. Average magnitude of  $\nu(t)$  taken across 500 realisations for each  $t_{max}$  for (a) the constrained and (b) reduced schemes with (green) and without (blue) the Wiener filter using  $\gamma = 0.01$ ,  $\beta = 1$ ,  $\Delta = 1$ ,  $\epsilon = -1$ ,  $\alpha = 0.05$  and  $\omega_c = 25$ .

#### D. Deconvolution and Causality

The instability of the direct Fourier division method can be observed by investigating the behaviour of the noises for different lengths of the simulation,  $t_{max}$ . We compare in Fig. 1 the stability of these two schemes with and without the Wiener filter, by observing the average magnitude of  $\nu(t)$  for different values of  $t_{max}$ . The application of the Wiener filter to the reduced and constrained noise schemes improves their stability enormously, in some cases by as much as an order of magnitude, and significantly weakens the erroneous dependence of  $\nu$  on  $t_{max}$ , though not removing it entirely. The trade-off for this improvement is a violation of the  $\eta$ - $\nu$  correlation function by introducing a breakdown of causality, as can be seen in Fig. 2.

The application of deconvolution methods thus successfully stabilizes the  $t_{max}$  dependence of  $\nu$ , decreasing its average magnitude by reducing the power of frequencies around the singularities in its spectral density. This improves the convergence and maximum possible run time of the dynamics, at the cost of weakening causality in the  $\eta$ - $\nu$  correlation. Weakening the Heaviside function or removing it entirely by hand also has this effect of smoothing the  $\nu$  noise and reducing the likelihood of realisations which contain atypically large values, in turn improving convergence.

While the causality of  $K_{\eta\nu}$  is a requirement of the theory, the introduction of the  $\gamma$  parameter gives us a method of deconvolution for which we can ensure any deviation from the theory is well controlled.

We have carried out tests of the above implementation of deconvolution. In Fig. 3 we show the dynamics of the  $z$ -spin  $\langle\sigma_z(t)\rangle$  with a constant Hamiltonian [the relaxation to the equilibrium case, Fig. 3(a)] and a Landau-Zener sweep [non-equilibrium case, Fig. 3(b)]. The Landau-Zener sweep consists of a linear driving of the form  $\epsilon(t) = \kappa t$ , and has a known analytic solution in the  $t \rightarrow \infty$  limit when the system was initialised in the ground state  $|1\rangle$  in the infinite past at zero temperature<sup>41</sup>. This limit is<sup>10,41–45</sup>

$$\langle\sigma_z\rangle_{LZ} = 2 \exp\left\{-\frac{\pi\Delta^2}{2\hbar\kappa}\right\} - 1,$$

and though originally derived for an isolated spin, it has since been shown that the same asymptotic behaviour is valid for a dissipative spin coupled to a harmonic environment at zero temperature, when the coupling is provided entirely via  $\sigma_z$ <sup>46</sup>. Note that this assumes that the system was initialised in the infinite past, whereas here it was initialised at  $t = -5$ . This is taken into account by modifying the limit appropriately<sup>18</sup>, though there is still some deviation associated with the fact that the bath is not at zero temperature and that the limit is asymptotic while the simulation time remains finite.

We expect to recover the canonical equilibrium state (associated with the constant Hamiltonian)<sup>18</sup> and the Landau-Zener limit as known solutions at long times in the two cases, and we investigate the constrained scheme with the Wiener filter for a range of  $\gamma$  values, using the  $\eta\nu$ -optimised scheme which minimises the sum of magnitudes of  $\eta$  and  $\nu$  as a reference. Without the Wiener filter ( $\gamma = 0$ ), the constrained scheme diverges almost immediately for both test cases, whereas for very small  $\gamma = 0.001$  there is already an improvement, with the accessible simulation time increasing by  $\sim 5$  times before  $\langle\sigma_z(t)\rangle$  diverges. Note that the behaviour of the  $z$ -spin after divergence is omitted for clarity as it oscillates wildly within an exponentially growing envelope. As  $\gamma$  increases to  $\sim 0.01$  and then to  $\sim 0.1$ , the constrained schemes begin to converge well, more closely resembling the  $\eta\nu$ -optimised scheme

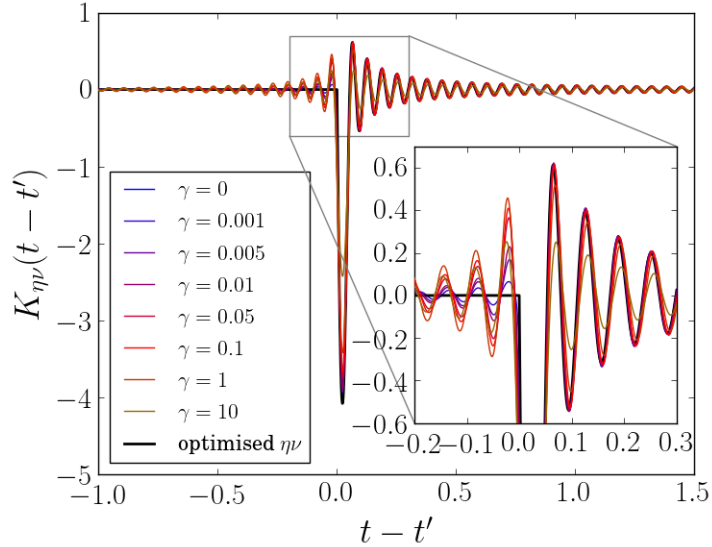


FIG. 2. The  $\eta$ - $\nu$  correlation function with different values of the parameter  $\gamma$  in the Wiener filter for the constrained noise scheme. the  $\eta\nu$  optimised scheme overlaps with the desired correlation  $K_{\eta\nu}$  such that  $K_{\eta\nu}$  could not be seen, so it is not shown.  $\beta = 1$ ,  $t_{max} = 12$ ,  $dt = 0.01$ ,  $\omega_c = 25$ ,  $\alpha = 0.05$  for  $10^4$  realisations. The zoomed inset highlights the region in which the symmetrisation of the correlation as  $\gamma$  increases can be clearly seen.

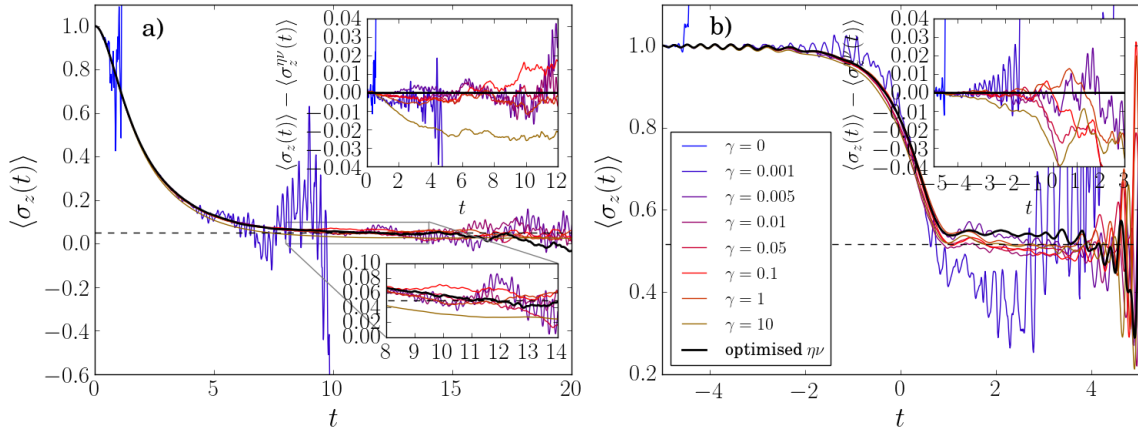


FIG. 3. Comparison of the calculated expectation of the  $z$ -spin  $\langle\sigma_z(t)\rangle$  using the constrained scheme with a range of  $\gamma$  values to control deconvolution, and the  $\eta\nu$ -optimised scheme  $\langle\sigma_z^{\eta\nu}(t)\rangle$ , which minimises the combined magnitude of  $\eta$  and  $\nu$ . (a) The system is initialised with the  $z$ -spin being 1 and all other spins being zero and is evolved in time with a constant Hamiltonian, so that the  $z$ -spin relaxes to its equilibrium value. The canonical equilibrium value of 0.05 for the spin, obtained using the imaginary time evolution methods outlined in<sup>18</sup>, is shown (dashed line) to confirm the validity of the optimised scheme. The inset shows the deviation of the  $z$ -spin for the constrained scheme from the optimised one. A zoomed-in area at the final stages of equilibration shows the  $z$ -spin in detail. (b) A Landau-Zener sweep with a time dependent Hamiltonian where the system is driven linearly with  $\epsilon(t) = 5t$ , approaching a known asymptotic limit (dashed line). The system is initialised at  $t = -5$  with the  $z$ -spin equal to 1 and all other spins being zero, using the modified Landau-Zener limit of 0.516 to account for the finiteness of the simulation window as outlined in<sup>18</sup>. For clarity, data are no longer plotted once they exceed the vertical scales shown, as the solution becomes unstable and grows exponentially.  $\beta = 0.1$ ,  $dt = 10^{-2}$ ,  $\Delta = 1$ ,  $\epsilon = -1$ ,  $\alpha = 0.05$  and  $\omega_c = 25$  for  $10^6$  realisations.

result  $\langle\sigma_z^{\eta\nu}(t)\rangle$  as can be seen in the insets of Fig. 3 where the difference between them is shown. The statistical convergence is best for larger values of  $\gamma$ , most noticeably for  $\gamma = 10$ , though such a strong Wiener filter introduces a significant deviation from the  $\eta\nu$ -optimised scheme and the known solutions, as can clearly be seen in both the inset and zoomed region in Fig. 3(a). The same is true in the non-equilibrium Landau-Zener case, Fig. 3(b), where for smaller  $\gamma$  the  $z$ -spin converges poorly while for larger  $\gamma$  it converges better at the expense of introducing a deviation from the solution used as a reference. Thus a compromise value of  $\gamma$  must be chosen.

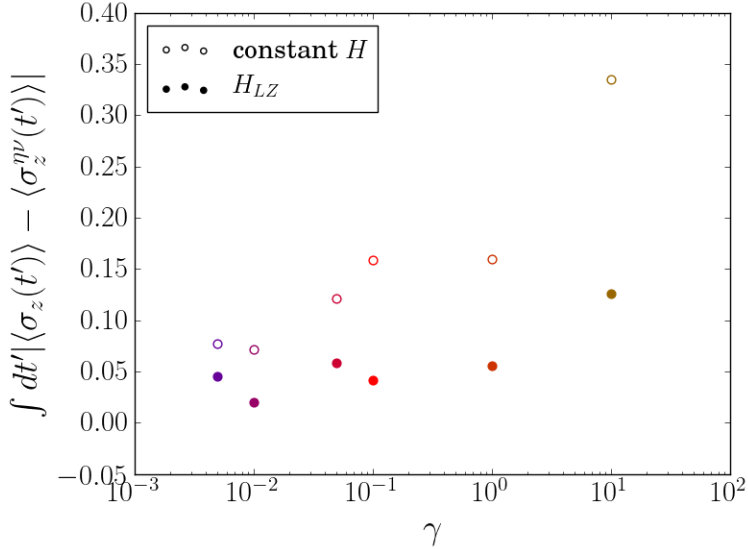


FIG. 4. The total absolute deviation of the dynamics produced using the constrained scheme for different  $\gamma$  from the dynamics produced using the  $\eta\nu$ -optimised scheme. Values were calculated using the data shown in the insets of Figs. 3(a) and (b). Results for  $\gamma = 0$  and 0.001 are not shown because the dynamics is diverging so the deviation is very large. The value of  $\gamma$  which minimises the total deviation for both the constant Hamiltonian (open circles, Fig. 3(a)) and the Landau-Zener sweep (filled circles, Fig. 3(b)) is 0.01.

The best  $\gamma$  value can be chosen by computing the integrated absolute deviation,  $\int dt' |\langle \sigma_z(t) \rangle - \langle \sigma_z^{\eta\nu}(t) \rangle|$ , for the data ranges shown in the insets of Fig. 3, presented in Fig. 4. This can be thought of as the total deviation from the  $\eta\nu$ -optimised scheme within the region where the convergence of the schemes are comparable, with results for  $\gamma = 0$  and 0.001 not shown since they do not remain well converged on useful timescales. The  $\gamma$  which minimises this quantity is the one with the smallest deviation from the correct dynamics which we find to be  $\gamma = 0.01$  for both the constant Hamiltonian and Landau-Zener cases. By minimising this deviation, we ensure that the breakdown of causality is well controlled while still managing to correctly handle the deconvolution and improve the convergence of the system properties.

## IV. RESULTS

### A. Verifying SLN Dynamics with a Quantum Non-Demolition Model

In this section, we verify the validity of the SLN equation by comparing the numerical results for  $\rho(t)$  simulated using the  $\eta\nu$ -optimised scheme with the analytical result obtained for a quantum non-demolition model<sup>47</sup>. The model considered<sup>6</sup> is a zero-temperature model with  $H_s = -\frac{1}{2}\sigma_z$ , the coupling to the environment is given by  $f = \sigma_z$ , and the environment's correlation function is taken to be  $K(t) = \frac{1}{2} \exp\{-2|t| + it\}$ . Since  $f$  and the Hamiltonian commute, the coupling can be thought of as an ideal projective measurement of the open system so as to not disturb its energy<sup>48</sup>. This model can be described exactly by the deterministic master equation<sup>4,49</sup>

$$i \frac{d\langle \rho(t) \rangle}{dt} = [H_s, \langle \rho(t) \rangle] - iC_r(t) [f, [f, \langle \rho(t) \rangle]] + C_i(t) [f^2, \langle \rho(t) \rangle], \quad (48)$$

where  $C_{r/i}(t) = \int_0^t d\tau K_{r/i}(t - \tau)$  with  $K_r(t) = \text{Re}[K(t)]$  and  $K_i(t) = \text{Im}[K(t)]$ . The analytical solution of Eq. (48) is easily found and can be compared to SLN dynamics computed numerically with any of the noise schemes we have considered above, and with correlations  $K_{\eta\eta} = \text{Re}[K(t)]$  and  $K_{\eta\nu} = 2i\text{Im}[K(t)]$ . The SLN dynamics using the  $\eta\nu$ -optimised scheme is shown in Fig. 5, along with the analytical solution of Eq. (48), using the initial condition  $\langle \rho(t_0) \rangle = 0.5I + 0.5\sigma_x + 0.6\sigma_y$ .

It is clear that the numerical simulation for a stochastic average of 50000 realisations matches the analytical solution for the real and imaginary parts of the density matrix element  $\langle \rho_{01}(t) \rangle$  very well. This off-diagonal element is rapidly damped to zero as the environment induces dephasing, with the SLN exhibiting good convergence beyond the

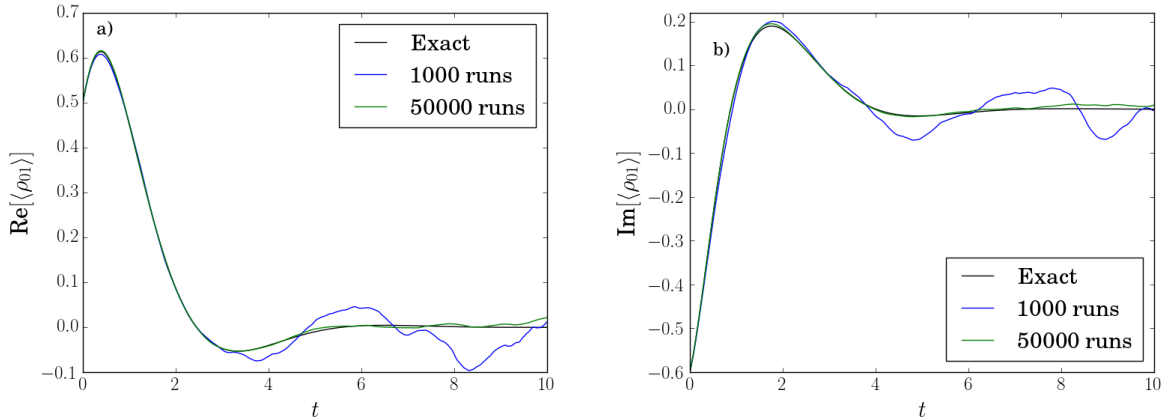


FIG. 5. Dynamics of the (01) element of the reduced density matrix according to the quantum non-demolition model, showing the real part  $\text{Re}[\langle \rho_{01}(t) \rangle]$  in (a), and the imaginary part  $\text{Im}[\langle \rho_{01}(t) \rangle]$  in (b). The exact solution (black line) is compared to the SLN numerical solutions for 1000 (blue line) and 50000 (green line) realisations, using the  $\eta\nu$ -optimised scheme with optimal scaling  $\lambda = 0.5$  (see Sec. IV C).

initial dephasing and into the equilibrium regime. Additionally, for a much smaller sample of only 1000 realisations, the SLN captures the exact dynamics well for short timescales  $t \lesssim 2$ . Having verified the validity of the SLN equation, in the next section we investigate the numerical efficiency of the noise schemes introduced in Section III.

## B. Error Control

The purpose of the optimisation schemes developed here is to minimise the typical amplitude of the  $\nu$  noise, since it drives the (potentially) exponential growth of the trace of the stochastic density matrix [Eq. (13)]. This should increase the accessible simulation time (after which convergence is destroyed by numerical blow up), and reduce the variance of observables.

Without some kind of optimisation, naive choices such as the delta scheme (Sec. III A 1) in which one of the components of  $\eta$  or  $\nu$  is purely white noise, tend to perform badly, or even be entirely pathological. The inclusion of white noise whose variance is one or two orders of magnitude greater than the trace  $\text{Tr}(\rho) \sim 1$  requires an excessive number of realisations  $\gtrsim 10^6$  for the correlation functions Eqs. (4)-(6) to converge<sup>17</sup>, though this by itself does not guarantee well behaved physical dynamics. Instead, the dynamics of the trace (or observables) is highly unstable even on very short timescales, being equally likely to diverge to  $+\infty$  as to  $-\infty$ . The physical average of such diverging observables will thus tend to zero as the white noise dominates the dynamics, effectively drowning out the coupling to the environment via the coloured noise. It is also clear that any attempt to normalise with the trace when an instability of this kind has occurred is inappropriate, requiring both division by zero as well as by very large numbers<sup>15,18</sup>. For these reasons we do not present any data for the delta scheme, and simply remark that this choice of noise generation scheme is entirely pathological and should not be used, providing an excellent illustration that it is not sufficient merely to satisfy the necessary correlation functions when driving systems using an SLN framework.

The other schemes all mark a drastic improvement on the naive delta scheme, as is seen from Fig. 6. Recall that the like scheme (Sec. III A 3) and constrained scheme (Sec. III A 2) represent the two distinguishing choices, where  $\eta$  and  $\nu$  have cross-correlated orthogonal components, or where all correlations are determined by  $f_1$  and  $g_1$  only, respectively. The optimised choices, barring convex optimisation, rely on weighting these choices to reduce the variance of the trace and extend the duration of stable dynamics.

Relative performance of the schemes is illustrated in Fig. 6, where we show the mean of the magnitude of the trace  $|\text{Tr}\rho(t)|$  [Figs. 6(a)-(c)], its variance [Figs. 6(d)-(f)], and the standard error of the mean [Figs. 6(g)-(i)] for all the schemes at three inverse temperatures,  $\beta = 0.1, 1, 10$ . In particular, the performance of the SLN can be quantified via the extent to which the behaviour of the average trace of the reduced density matrix remains constant and close to unity, indicating that the dynamics are physical and well converged, shown in Figs. 6 (a)-(c). The physical situation is the same as in Fig. 3(a), where the system is initialised in the state  $|1\rangle$  with the  $z$ -spin equal to 1 and all other spins being zero and relaxes towards the equilibrium state associated with a constant Hamiltonian.

In general, either of the optimised schemes represent a very significant improvement in the convergence properties

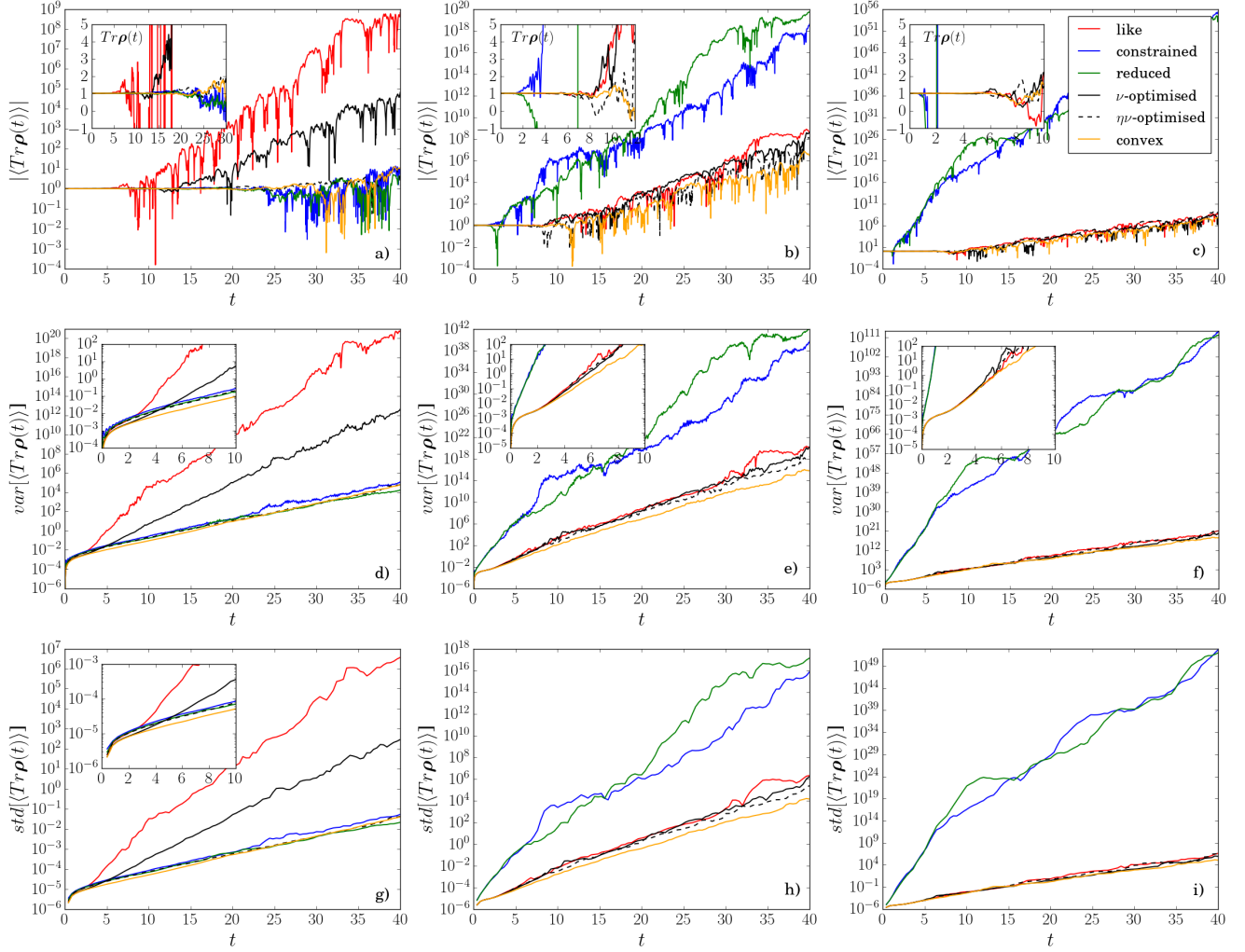


FIG. 6. (a)-(c): The mean value of the trace,  $\langle \text{Tr}(\rho(t)) \rangle$ , calculated using different schemes with the system having been initialised in the state  $|1\rangle$  for a constant Hamiltonian. The absolute value of  $\langle \text{Tr}(\rho(t)) \rangle$  is shown so that the linear growth on a logarithmic scale is clear. The insets highlight the timescales on which the simulation is numerically stable, showing  $\langle \text{Tr}(\rho(t)) \rangle$  directly; schemes are not shown for timescales beyond which the trace is clearly diverging. (d)-(f): The variance of the trace and (g)-(i): the standard error of the mean trace calculated over time windows which were 100 time steps long. For columns read from left to right, the inverse temperature increases as  $\beta = 0.1, 1, 10$ , respectively. The like (red), constrained (blue) and reduced (green) schemes are shown, as well as the  $\nu$ -optimised scheme which minimises  $\langle |\nu(t)|^2 \rangle$  (black solid),  $\eta\nu$ -optimised scheme which minimises the sum  $\langle |\eta(t)|^2 \rangle + \langle |\nu(t)|^2 \rangle$  (black dashed), and the application of the convex optimisation scheme<sup>21</sup> as implemented using Eqs. (37)–(42) (yellow). All calculations have been done using the same system as in Fig. 3(a).  $\Delta = 1$ ,  $\epsilon = -1$ ,  $\alpha = 0.05$ ,  $\Delta t = 10^{-2}$ ,  $\omega_c = 25$  and  $10^5$  realisations. No rescaling of the noises was employed.

and stability of the trace for the inverse temperatures used, with the growth in the variance of the trace being drastically reduced [Figs. 6(d)-(f)], allowing an increase in the duration of the stable region [Figs. 6(a)-(c)]. However, minimising the typical magnitude of  $\nu$  only is found not sufficient to guarantee this reduction in the variance of the trace for all temperatures, with the performance of the  $\nu$ -optimised scheme only similar to the  $\eta\nu$ -optimised and convex optimised schemes at lower temperatures ( $\beta = 1, 10$ ), but performing much worse at high temperatures ( $\beta = 0.1$ ).

This is understood by comparing Figs. 6(d) and (f) for the variance, where the  $\nu$ -optimised scheme and the like scheme both fail for small  $\beta$  while the  $\eta\nu$ -optimised scheme performs well. This is caused by the presence of  $\coth(\frac{1}{2}\beta\hbar\omega)$  in  $K_{\eta\eta}$  [Eq. (4)] which diverges as  $\beta$  becomes small. Since correlation of  $\nu$  with  $\eta$  enters via the autocorrelative part of  $\eta$  in the reduced scheme, the amplitude of  $\eta$  when generated by the reduced scheme will be smaller than when generated by the like scheme, as no other noise component is added to the autocorrelative part. This also explains why the reduced and constrained schemes perform well for  $\beta = 0.1$  [Figs. 6(a), (d) and (g)]. By

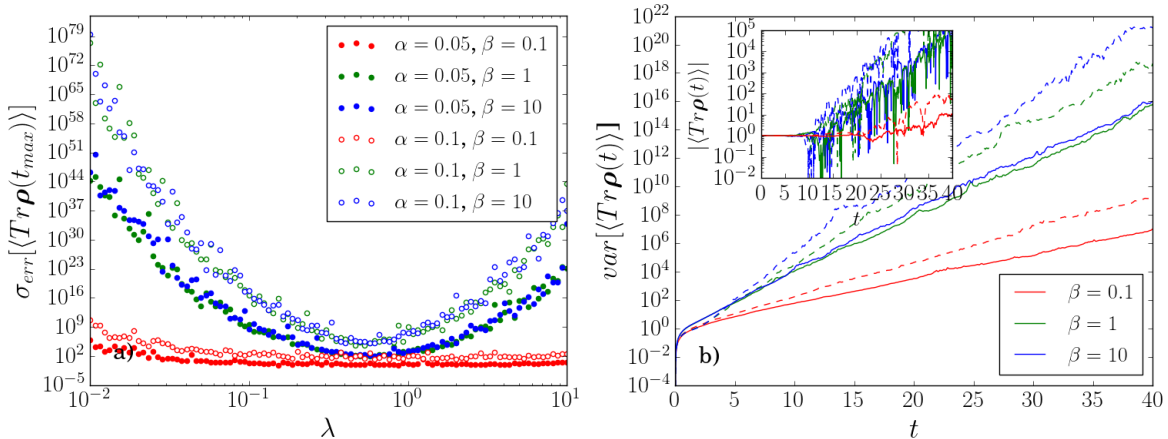


FIG. 7. (a) The standard error of  $\langle \text{Tr} \rho(t) \rangle$  at its final time step  $t_{max}$  as a function of the scaling factor  $\lambda$  for several values of inverse temperature  $\beta$  and coupling strength  $\alpha$ . For each scaling factor, 1000 runs for real time dynamics were performed.  $t_{max} = 40$ ,  $dt = 10^{-3}$ ,  $\omega_c = 25$  and  $\Delta = 1$ ,  $\epsilon = -1$  for  $\alpha = 0.05, 0.1$  and  $\beta = 0.1, 1, 10$ . In this case, the optimum value of  $\lambda$  which minimises the growth of the trace is  $\approx 0.5$ . (b) The variance of the trace having used the  $\eta\nu$ -optimised scheme with scaling, with a desired ratio between  $f_2(t)$  and  $g_2(t)$  of  $\lambda = 0.5$  (solid lines) for  $\beta = 0.1, 1, 10$ , with the mean trace shown in the inset. The convex optimised scheme (dashed lines) has been reproduced here from Fig. 6(d)-(f) for comparison.

accounting for this, the  $\eta\nu$ -optimised scheme is an improvement on the  $\nu$ -optimised scheme despite the fact that  $\nu$  alone is responsible for the intrinsic exponential growth of the trace; this acts as a reminder that these optimisation schemes are indirect, in the sense that they do not optimise the properties of the dynamics of the trace directly.

Accounting for this temperature dependence, the raw  $\eta\nu$ -optimised scheme (without any rescaling) and the application of convex optimisation are comparable, with the benefit that these schemes are universal rather than depending strongly on the temperature. It is quite fortunate, as if this were not the case, an investigation of this kind would have to be performed for every system when selecting a scheme.

### C. $\eta\nu$ -Optimised Scheme with Rescaling

In Fig. 7 we apply dynamical scaling to the  $f_2$  and  $g_2$  components of  $\eta$  and  $\nu$  as generated by the  $\eta\nu$ -optimised scheme, Eqs. (33)-(35), with  $\zeta = 1/2$ . By comparing in Fig. 7(a) the value of  $|\langle \text{Tr} \rho(t) \rangle|$  at the end of a constant Hamiltonian simulation for a range of rescaling values  $\lambda \in (0.01, 10)$  using the procedure of Sec. III A 6, we find that the optimal value of the scaling is  $\lambda = 0.5$ , which we note is the same value obtained previously for the like scheme<sup>18</sup>. Rescaling the noises with this optimal  $\lambda$  using the same parameters as in Fig. 6, we find that the variance of the trace is reduced further, shown in Fig. 7(b) alongside the convex optimised data from Fig. 6 for comparison.

We find that the rescaled  $\eta\nu$ -optimised scheme is the best scheme for generating noises which minimise the spread and growth (see inset) of the trace for all the schemes considered, at both high and low temperatures. From a practical perspective, the optimal  $\lambda$  can be quickly obtained with only 100 realisations or fewer for each value of  $\lambda$ , so does not represent a meaningful increase in computational effort.

## V. DISCUSSION AND CONCLUSIONS

In this paper we have developed a number of competing noise generation schemes, capable of generating complex coloured noises appropriate for the implementation of the Stochastic Liouville-von Neumann equation. These noises represent the interaction between the system of interest and its environment and must satisfy the correlation functions of Eqs. (4) and (5), with the physical interpretation that averaging over the manifestations of these noises is equivalent to averaging over all possible behaviours of the bath. All of the schemes proposed here do satisfy the desired correlations, but do not otherwise perform equally; that is, the required sample size for convergence is not uniform between schemes, and nor is the quality of the subsequent driven dynamics of the reduced system density matrix. This leads to the important point that there is significant flexibility in the definitions of the noises, as they are not uniquely defined by the correlation functions which they must satisfy.

At all stages in this work, great care has been taken to be as transparent and explicit in the development as

possible, in terms of both the presentation of analytical solutions and the numerical implementation of the schemes subsequently developed.

Within the general linear filtering ansatz [Eqs. (14) and (15)] we have identified a sub-class of schemes, which we refer to as orthogonal decompositions<sup>17</sup>, where the noises are decomposed into components which are correlated only with one other component (or with themselves), and have the beneficial property that zero self-correlation can be fulfilled by construction. There is no limit to the possible choices of the filters with which these components might be generated from white noise, though we focus on two such choices for the cross-correlative components between the  $\eta$  and  $\nu$  noises: the delta scheme (Sec. III A 1) where one of the noise components is chosen to be purely white noise, and the like scheme (Sec. III A 3) where the filters are chosen so that one is equal to the other with  $\omega \rightarrow -\omega$ . The delta scheme represents the worst of the choices, requiring sample sizes of at least  $\sim 10^6$  for the correlation functions to converge while still producing unstable dynamics for which the trace rapidly diverges to  $\pm\infty$ . This is a prime demonstration that satisfying the correlation functions alone is not sufficient to guarantee well-behaved dynamics, or that unrealistically large samples might be required before the dynamics converges.

Building on an alternative structure for the noises which cannot be written as an orthogonal decomposition, we followed the arguments in Ref.<sup>20</sup> to develop a scheme which chooses either the like or constrained scheme (of Secs. III A 3 and III A 2, respectively) at each  $\omega$  to reduce the average magnitude of the  $\nu$  noise which controls the spreading of the trace of the reduced system density matrix. Crucially, by introducing a mixing function  $\tilde{A}(\omega)$  to blend the schemes and performing a minimisation in Fourier space to choose it, we were able to ensure that the mixing function was introduced to the filters in Eqs. (27)-(29) correctly such that the properties of the Fourier transforms of the correlation functions were maintained. Further, by exploiting these properties and deriving the Fourier transforms in full, we were able to identify that the enforcement of causality in the  $\eta$ - $\nu$  correlation was responsible for a logarithmic divergence in its Fourier transform. This in turn causes an amplification of the noise power for frequencies around the cutoff frequency of the spectral density of the bath, resulting in weaker convergence than if causality was not required. Fortunately, by employing the Wiener filter for deconvolutions in Sec. III C, we were able to parametrise a weakening of causality in cases where division by zero (or very small numbers) in Fourier space would cause the spectral densities of the noises to diverge, ensuring that any deviation from the theory was well controlled while significantly reducing the  $\nu$  noise power.

Going one step further, we explicitly minimised the average amplitude of both the  $\nu$  noise, and the combined amplitudes of the  $\eta$  and  $\nu$  noises together, in the  $\nu$ -optimised and  $\eta\nu$ -optimised schemes, respectively. We then exploited an additional freedom in the relative amplitudes of correlated noise components by increasing the noise power of one component while reducing the noise power of the other by the same amount so that the correlation functions are unchanged. We showed that analytic minimisation of the amplitudes of the noises yields a trivial rescaling, but that direct numerical minimisation of the standard error of the trace allows us to obtain an optimal scaling. We emphasise that this scaling is an entirely independent freedom to the mixing function, and suggest that there may be many other freedoms and equivalent noise constructions, leaving space for future work.

Finally, we measured the performance of the aforementioned schemes along with an alternative optimised scheme (Sec. III B) based on convex optimisation<sup>21</sup> for a range of inverse temperatures, paying special attention to the properties of the reduced system trace as a measure of the deviation from the physical dynamics, as well as its convergence over a set of realisations. By measuring the variance and standard error of the mean of the trace, and inspecting how the time at which numerical breakdown occurs varies for each scheme, we were able to explain why some schemes performed better at different temperatures than others in terms of competing noise amplitudes between  $\eta$  and  $\nu$ , and clearly identified that the re-scaled  $\eta\nu$ -optimised scheme performed universally the best out of all the schemes at all temperatures. Remarkably, this optimisation reduced the variance of the trace by as much as  $\sim 10^{95}$  at low temperatures and  $\sim 10^{15}$  at high temperatures. The SLN equation is then compared with the exact solution of a simple quantum non-demolition model, for which near perfect agreement is obtained with statistical convergence extending beyond initial dynamics and into the equilibrium regime.

While comparison with other methods was not within the scope of this paper, we remark that methods which use approximate forms of the bath response function and do not rely so heavily on noises, eg, the hierarchical equations of motions<sup>5,8</sup>, achieve well converged results for strong coupling. However, for weaker coupling or arbitrary spectral densities and bath response functions the SLN remains exact, opening an avenue of research for non-Markovian reservoir engineering<sup>50,51</sup>. We hope that this study will stimulate further work in improving the optimisation of the simulation schemes and consequently will open avenues for practical numerical simulations of open quantum systems using SLN and ESLN approaches.

## ACKNOWLEDGEMENTS

The first two authors contributed equally to this work. D.M and M.A.L are supported by the EPSRC Centre for Doctoral Training in Cross-Disciplinary Approaches to Non-Equilibrium Systems (CANES, Grant No.

## APPENDICES

### Appendix A: Fourier Transforms

In deriving the different noise generation schemes (Sec. III), it was necessary to use the properties of the Fourier transform of the  $\eta - \eta$  correlation function  $K_{\eta\eta}(t)$  and the  $\eta - \nu$  correlation function  $K_{\eta\nu}(t)$  which we reproduce here.

#### 1. $\tilde{K}_{\eta\eta}(\omega)$

Recalling the definition of  $K_{\eta\eta}(t)$  (Eq. (4)), its Fourier transform  $\tilde{K}_{\eta\eta}(\omega)$  is

$$\tilde{K}_{\eta\eta}(\omega) = \frac{\hbar}{2} \int_{-\infty}^{\infty} dt \int_0^{\infty} \frac{d\omega'}{\pi} \Lambda(\omega') \left[ e^{-i(\omega-\omega')t} + e^{-i(\omega+\omega')t} \right], \quad (\text{A.1})$$

where we have used the shorthand  $\Lambda(\omega) = J(\omega) \coth(\frac{1}{2}\beta\hbar\omega)$  and replaced the cosine with complex exponentials. Using the definition of the  $\delta$  function to remove the time integral,

$$\delta(\omega) = \frac{1}{2\pi} \int_{-\infty}^{\infty} dt e^{\pm i\omega t}, \quad (\text{A.2})$$

we arrive at the final result,

$$\tilde{K}_{\eta\eta}(\omega) = \hbar \int_0^{\infty} d\omega' \Lambda(\omega') [\delta(\omega - \omega') + \delta(\omega + \omega')] = \hbar \Lambda(|\omega|), \quad (\text{A.3})$$

and we can see that  $\tilde{K}_{\eta\eta}(\omega)$  is both real, even and everywhere positive.

#### 2. $\tilde{K}_{\eta\nu}(\omega)$

Recalling the definition of  $K_{\eta\nu}(t)$ , Eq. (5), its Fourier transform  $\tilde{K}_{\eta\nu}(\omega)$  is

$$\tilde{K}_{\eta\nu}(\omega) = \frac{1}{2i\pi} \int_0^{\infty} \frac{d\omega'}{\pi} J(\omega') \lim_{\epsilon \rightarrow 0^+} \int_{-\infty}^{\infty} \frac{d\Omega}{\Omega + i\epsilon} \int_{-\infty}^{\infty} dt \left[ e^{-i(\omega+\Omega-\omega')t} - e^{-i(\omega+\Omega+\omega')t} \right], \quad (\text{A.4})$$

where we have replaced the Heaviside step function with

$$\Theta(t) = \lim_{\epsilon \rightarrow 0^+} -\frac{1}{2i\pi} \int_{-\infty}^{\infty} d\Omega \frac{e^{-i\Omega t}}{\Omega + i\epsilon}, \quad (\text{A.5})$$

and replaced the sine with complex exponentials. Again, recognising the definition of the  $\delta$  function, Eq. (A.2), to remove the time integral and then using the  $\delta$  functions to evaluate the  $\Omega$  integral, we arrive at the following,

$$\tilde{K}_{\eta\nu}(\omega) = -i \lim_{\epsilon \rightarrow 0^+} \int_0^{\infty} \frac{d\omega'}{\pi} J(\omega') \left[ \frac{1}{\omega' - \omega + i\epsilon} + \frac{1}{\omega' + \omega - i\epsilon} \right]. \quad (\text{A.6})$$

We then take the  $\epsilon \rightarrow 0^+$  limit to remove the pole,

$$\lim_{\epsilon \rightarrow 0^+} \frac{1}{\omega' - \omega \pm i\epsilon} = \mathcal{P} \frac{1}{\omega' - \omega} \mp i\pi \delta(\omega' - \omega), \quad (\text{A.7})$$

( $\mathcal{P}$  stands for Cauchy principal value) to obtain

$$\tilde{K}_{\eta\nu}(\omega) = \int_0^{\infty} d\omega' J(\omega') [\delta(\omega' + \omega) - \delta(\omega' - \omega)] - \frac{i}{\pi} \int_0^{\infty} d\omega' J(\omega') \left( \frac{1}{\omega' - \omega} + \frac{1}{\omega' + \omega} \right) \quad (\text{A.8})$$

$$= -\text{sgn}(\omega)J(|\omega|) - \frac{2i}{\pi} \int_0^\infty d\omega' \frac{\omega' J(\omega')}{\omega'^2 - \omega^2}, \quad (\text{A.9})$$

where  $f$  also corresponds to Cauchy principal value. Note that  $\tilde{R}(\omega) = -i\tilde{K}_{\eta\nu}(\omega)$ , so we immediately see that the real part of  $\tilde{K}_{\eta\nu}$  (and the imaginary part of  $\tilde{R}$ ) is odd.

### 3. The singularity in $\tilde{K}_{\eta\nu}(\omega)$

From Eq. (A.9), we see that the imaginary part of  $\tilde{K}_{\eta\nu}(\omega)$  has an instability at  $\omega' = \omega$  that is integrable due to the Cauchy principle value. By writing  $\text{Im} [\tilde{K}_{\eta\nu}(\omega)]$  as

$$\text{Im} [\tilde{K}_{\eta\nu}(\omega)] = -\frac{2}{\pi} \int_0^{\omega_c} d\omega' \frac{\omega'^2 f(\omega')}{\omega'^2 - \omega^2}, \quad (\text{A.10})$$

where  $f(\omega) = \left[1 + \left(\frac{\omega}{\omega_c}\right)^2\right]^{-2}$  and we have used the fact that  $J(\omega)$  is zero outside of the range of  $\omega$  values  $0 \leq \omega \leq \omega_c$ , we integrate it as follows:

$$\int_0^{\omega_c} dx \frac{x^2 f(x)}{x^2 - \omega^2} = \int_0^{\omega_c} dx \frac{x^2 [f(x) - f(\omega)]}{x^2 - \omega^2} + f(\omega) \int_0^{\omega_c} dx \frac{x^2}{x^2 - \omega^2}. \quad (\text{A.11})$$

Only the second term contains the instability which can be handled as

$$\int_0^{\omega_c} dx \frac{x^2}{x^2 - \omega^2} = \int_0^{\omega_c} dx + \omega^2 \int_0^{\omega_c} \frac{dx}{x^2 - \omega^2} = \omega_c + \frac{\omega}{2} \ln \left| \frac{\omega_c - \omega}{\omega_c + \omega} \right| \quad (\text{A.12})$$

by breaking the Cauchy principal value integral into an integral from 0 to  $\omega - \epsilon$  and from  $\omega + \epsilon$  to  $\omega_c$  and seeing that the result is independent of the infinitesimal  $\epsilon$ . Hence Eq. (A.11) converges in the Cauchy sense, though a logarithmic divergence at  $\omega = \pm\omega_c$  has appeared.

Applying this argument to  $\text{Im} [\tilde{K}_{\eta\nu}(\omega)]$  and simplifying, we arrive at

$$\begin{aligned} \text{Im} [\tilde{K}_{\eta\nu}(\omega)] &= -\frac{2}{\pi} \left( \omega_c + \frac{\omega}{2} \ln \left| \frac{\omega_c - \omega}{\omega_c + \omega} \right| \right) f(\omega) \\ &+ \frac{2}{\pi} \frac{\omega_c^3}{\omega_c^2 + \omega^2} \int_0^1 dx \frac{x^2}{(1+x^2)^2} [\omega_c^2 x^2 + 2\omega_c^2 + \omega^2]. \end{aligned} \quad (\text{A.13})$$

The remaining integrals are then evaluated by relation to the arctangent to give

$$\begin{aligned} \text{Im} [\tilde{K}_{\eta\nu}(\omega)] &= -\frac{2}{\pi} \left( \omega_c + \frac{\omega}{2} \ln \left| \frac{\omega_c - \omega}{\omega_c + \omega} \right| \right) \left[ 1 + \left( \frac{\omega}{\omega_c} \right)^2 \right]^{-2} \\ &+ \frac{1}{4\pi} \frac{\omega_c^3}{(\omega_c^2 + \omega^2)} [(6 - \pi)\omega_c^2 + (\pi - 2)\omega^2]. \end{aligned} \quad (\text{A.14})$$

Thus the imaginary part of  $\tilde{K}_{\eta\nu}$  is even and the real part of  $\tilde{R}$  is odd.

The emergence of the logarithmic divergence when  $\omega = \pm\omega_c$  originates with the presence of the Heaviside step function in the  $\eta\nu$  correlation of Eq. (5), which by Eq. (A.5) and the use of the  $\delta$  function introduces the singularity  $\sim \frac{1}{\omega'^2 - \omega^2}$  in Eq. (A.9). Since the Heaviside function is an intrinsic part of the  $\eta\nu$  correlation, that is, it was rigorously derived<sup>16</sup> rather than being included artificially, its presence is required by the theory such that removing it any way would not be formally correct.

## Appendix B: Optimised Mixing Function $\tilde{A}(\omega)$

### 1. Symmetry of $\tilde{A}(\omega)$

It is possible to determine some general properties of the real and imaginary parts of the mixing function  $\tilde{A}(\omega) = \tilde{A}_1(\omega) + i\tilde{A}_2(\omega)$  simply from the properties of  $\tilde{R}$ . Recalling Eq. (20) coming from  $\tilde{K}_{\eta\nu}$  and generalising to arbitrarily many cross correlative components,

$$\tilde{f}_1(\omega)\tilde{g}_1(-\omega) + 2 \sum_{j=2} \tilde{f}_j(\omega)\tilde{g}_j(-\omega) = \tilde{R}(\omega), \quad (\text{B.1})$$

we can then make use of the fact that  $\{f_j(t)\}$  and  $\{g_j(t)\}$  are all real functions. Thus their Fourier transforms must have even real parts and odd imaginary parts, since  $\tilde{f}^*(\omega) = \tilde{f}(-\omega)$  for any real function  $f(t)$ . Then, from Eqs. (A.9) and (A.14), we see that  $\tilde{R}(\omega) = \tilde{R}_1(\omega) + i\tilde{R}_2(\omega)$  has even real part  $\tilde{R}_1$  and odd imaginary part  $\tilde{R}_2$ . Using the shorthand  $\tilde{f}_j = \tilde{f}_j^R + i\tilde{f}_j^I$  and  $\tilde{g}_j = \tilde{g}_j^R + i\tilde{g}_j^I$  for the real and imaginary parts of the filters, we thus have

$$\tilde{R}_1(\omega) = \sqrt{\tilde{K}_{\eta\eta}(\omega)}\tilde{g}_1^R(\omega) + 2 \sum_{j=2} \left[ \tilde{f}_j^R(\omega)\tilde{g}_j^R(\omega) + \tilde{f}_1^I(\omega)\tilde{g}_j^I(\omega) \right], \quad (\text{B.2})$$

for the real part, where we have used the fact that the real parts of the filters are even and that the imaginary parts are odd, and that  $\tilde{f}_1(\omega) = \sqrt{\tilde{K}_{\eta\eta}(\omega)}$  is real. Similarly for the imaginary part we have

$$\tilde{R}_2(\omega) = \sqrt{\tilde{K}_{\eta\eta}(\omega)}\tilde{g}_1^I(\omega) + 2 \sum_{j=2} \left[ \tilde{f}_j^R(\omega)\tilde{g}_j^I(\omega) - \tilde{f}_j^I(\omega)\tilde{g}_j^R(\omega) \right]. \quad (\text{B.3})$$

For the case we are considering where we include only the  $j = 2$  term, and using the filters given by Eqs. (26)-(29), we can determine the symmetry properties of the real and imaginary parts of the mixing function  $\tilde{A}(\omega) = \tilde{A}_1(\omega) + i\tilde{A}_2(\omega)$ . Since  $\tilde{g}_1(-\omega) = \tilde{g}_1^*(\omega)$ , the general  $\tilde{g}_1$  filter requires

$$\left[ 1 - \tilde{A}_1(\omega) - i\tilde{A}_2(\omega) \right] \left[ \tilde{R}_1(\omega) + i\tilde{R}_2(\omega) \right] = \left[ 1 - \tilde{A}_1(-\omega) + i\tilde{A}_2(-\omega) \right] \left[ \tilde{R}_1(-\omega) - i\tilde{R}_2(-\omega) \right], \quad (\text{B.4})$$

which constrains the real and imaginary parts as

$$\left[ \tilde{A}_1(\omega) - \tilde{A}_1(-\omega) \right] \tilde{R}_1(\omega) = \left[ \tilde{A}_2(\omega) + \tilde{A}_2(-\omega) \right] \tilde{R}_2(\omega) \quad (\text{B.5})$$

$$- \left[ \tilde{A}_1(\omega) - \tilde{A}_1(-\omega) \right] \tilde{R}_2(\omega) = \left[ \tilde{A}_2(\omega) + \tilde{A}_2(-\omega) \right] \tilde{R}_1(\omega) \quad (\text{B.6})$$

respectively, where we have again used the symmetry properties of  $\tilde{R}$ . Assuming that  $\tilde{A}_1(\omega) - \tilde{A}_1(-\omega) \neq 0$ , then  $\tilde{A}_2(\omega) + \tilde{A}_2(-\omega) \neq 0$  and dividing Eq. (B.5) by (B.6) would require that  $\tilde{R}_1(\omega)^2 = -\tilde{R}_2(\omega)^2$  which is obviously incorrect since they are both real. Therefore  $\tilde{A}_1(\omega) = \tilde{A}_1(-\omega)$  and then  $\tilde{A}_2(\omega) = -\tilde{A}_2(-\omega)$ , i.e. the real part of the mixing function must be even and the imaginary part must be odd.

Note that the same analysis of Eqs. (27) and (29) results in exactly the same conditions for the mixing function.

### 2. Minimising magnitude of $\nu(t)$

Starting with  $\nu$  as it is written in Eq. (17), its magnitude is

$$\langle |\nu(t)|^2 \rangle = \int \frac{d\omega}{2\pi} \tilde{K}_{\nu\nu^*}(\omega) = \int \frac{d\omega}{2\pi} (2|\tilde{g}_1(\omega)|^2 + 2|\tilde{g}_2(\omega)|^2), \quad (\text{B.7})$$

where  $K_{\nu\nu^*}(t) = \langle \nu(t) \nu^*(t) \rangle$  and we have made use of Parseval's theorem to remove the exponential factor associated with the inverse Fourier transform. While it may at first seem strange that there is no time dependence on the right hand side, there is no reason why  $\langle |\nu(t)|^2 \rangle$  should not be stationary. In fact, this apparent stationarity is a direct consequence of the form of the noises Eqs. (16) and (17) containing time differences in the filters. Substituting in the above expression Eqs. (28) and (29) and making use of the fact that  $\tilde{K}_{\eta\eta}(\omega)$  is real and even, that the real part of  $\tilde{R}(\omega) = \tilde{R}_1(\omega) + i\tilde{R}_2(\omega)$  is even while the imaginary part is odd, we obtain Eq. (30) for  $\langle |\nu(t)|^2 \rangle$ . We have also used the fact that the magnitude of a complex function whose real and imaginary parts are either even or odd is always real, even and positive. The aim now is to minimise  $\tilde{K}_{\nu\nu^*}(\omega)$  with respect to the real and imaginary parts of the mixing function  $\tilde{A}(\omega) = \tilde{A}_1(\omega) + i\tilde{A}_2(\omega)$  at each  $\omega$  value, where we know that the real part of  $\tilde{A}$  should be even and the imaginary part odd. Starting with the real part,

$$\frac{d\tilde{K}_{\nu\nu^*}(\omega)}{d\tilde{A}_1(\omega)} = \frac{|\tilde{R}(\omega)|}{\tilde{K}_{\eta\eta}(\omega)} \left[ 4|\tilde{R}(\omega)| + \tilde{K}_{\eta\eta}(\omega) \frac{\tilde{A}_1(\omega)}{|\tilde{A}(\omega)|} \right] = 0, \quad (\text{B.8})$$

which yields the following constraint on  $\tilde{A}_1$  and its magnitude,

$$\tilde{A}_1(\omega) \left[ 4|\tilde{R}(\omega)| + \frac{\tilde{K}_{\eta\eta}(\omega)}{|\tilde{A}(\omega)|} \right] = 4|\tilde{R}(\omega)|. \quad (\text{B.9})$$

Minimising with respect to the imaginary part of the mixing function then gives

$$\frac{d\tilde{K}_{\nu\nu^*}(\omega)}{d\tilde{A}_2(-\omega)} = \frac{|\tilde{R}(\omega)|}{\tilde{K}_{\eta\eta}(\omega)} \tilde{A}_2(-\omega) \left[ 4|\tilde{R}(\omega)| + \frac{\tilde{K}_{\eta\eta}(\omega)}{|\tilde{A}(-\omega)|} \right] = 0, \quad (\text{B.10})$$

so that  $\tilde{A}$  must either be real with  $\tilde{A}_2(\omega) = 0$ , or the terms within the square brackets must equal zero. If the latter was true, then Eq. (B.9) would require that  $|\tilde{R}(\omega)| = 0$  which is certainly not correct (also, both terms inside the square brackets are positive), so  $\tilde{A}$  is indeed real,  $\tilde{A}(\omega) = \tilde{A}_1(\omega)$ . Equation (B.9) then gives

$$\tilde{A}(\omega) = 1 - \text{sgn}(\tilde{A}(\omega)) \frac{\tilde{K}_{\eta\eta}(\omega)}{4|\tilde{R}(\omega)|}. \quad (\text{B.11})$$

Since  $\tilde{A} < 0$  would lead to a contradiction ( $\tilde{K}_{\eta\eta}/|\tilde{R}|$  is always positive, so the right hand side would then be positive), we must conclude that  $\tilde{A}$  is a positive function, leading finally to

$$\tilde{A}(\omega) = 1 - \frac{\tilde{K}_{\eta\eta}(\omega)}{4|\tilde{R}(\omega)|}. \quad (\text{B.12})$$

Substituting this  $\tilde{A}$  into the filters of Eqs. (27)-(29) gives Eqs. (33)-(35). It is worth noting that the division by  $|\tilde{R}(\omega)|$  does not require serious consideration using the deconvolution procedure as detailed in Sec. (III C) since it appears as only a combination  $\tilde{R}(\omega)/|\tilde{R}(\omega)|$ . Since  $|\tilde{R}| \geq \tilde{R}$ , this ratio will always converge without any division by small numbers.

### 3. Minimising magnitudes of $\eta(t)$ and $\nu(t)$

We now consider the sum

$$\langle |\eta(t)|^2 \rangle + \langle |\nu(t)|^2 \rangle = \int \frac{d\omega}{2\pi} \left( \tilde{K}_{\eta\eta}(\omega) + \tilde{K}_{\nu\nu^*}(\omega) \right)$$

$$= \int \frac{d\omega}{2\pi} \left( \tilde{f}_1(\omega)^2 + 2|\tilde{f}_2(\omega)|^2 + 2|\tilde{g}_1(\omega)|^2 + 2|\tilde{g}_2(\omega)|^2 \right), \quad (\text{B.13})$$

and insert Eqs. (26)-(29) to obtain

$$\tilde{K}_{\eta\eta}(\omega) + \tilde{K}_{\nu\nu^*}(\omega) = \tilde{K}_{\eta\eta}(\omega) + 2 \left| \tilde{R}(\omega) \right| \left| \tilde{A}(\omega) \right| + 2 \frac{|\tilde{R}(\omega)|^2}{\tilde{K}_{\eta\eta}(\omega)} \left| 1 - \tilde{A}(\omega) \right|^2, \quad (\text{B.14})$$

where we have again used the properties of  $\tilde{K}_{\eta\eta}$  and  $\tilde{R}$ , and the fact that  $\tilde{A}$  must be an even function. The essential difference of the obtained expression from Eq. (30) for  $\langle |\nu(t)|^2 \rangle$  is only in the factor of two in the last term. Hence, repeating the analysis of the previous Appendix we obtain

$$\tilde{A}(\omega) = 1 - \frac{\tilde{K}_{\eta\eta}(\omega)}{2|\tilde{R}(\omega)|}. \quad (\text{B.15})$$

Note that the same result can be obtained without initially using the fact that  $\tilde{A}$  is an even function, in which case it is more convenient to write  $\tilde{A}$  in the form  $\tilde{A}(\omega) = r(\omega) e^{i\theta(\omega)}$ .

- 
- <sup>1</sup> P. W. Shor. Scheme for reducing decoherence in quantum computer memory. *Phys. Rev. A* 52, R2493 (1995).
- <sup>2</sup> U. Weiss. *Quantum dissipative systems* (World scientific, Singapore, 2012), Vol. 13.
- <sup>3</sup> R. P. Feynman and F. L. Vernon Jr. The theory of a general quantum system interacting with a linear dissipative system. *Annals of physics* 281, 547 (2000).
- <sup>4</sup> J. Shao. Decoupling quantum dissipation interaction via stochastic fields. *Chemical physics* 120, 5053 (2004).
- <sup>5</sup> Y. Yan, F. Yang, Y. Liu, and J. Shao. Hierarchical approach based on stochastic decoupling to dissipative systems. *Chem. Phys. Lett* 395, 216 (2004).
- <sup>6</sup> Y.A. Yan, and J. Shao. Stochastic description of quantum Brownian dynamics. *Frontiers of Physics* 11, 110309 (2016).
- <sup>7</sup> Y. Zhou, Y. Yan, and J. Shao. Stochastic simulation of quantum dissipative dynamics. *EPL* 72, 334 (2005).
- <sup>8</sup> Y. Zhou, and J. Shao. Solving the spin-boson model of strong dissipation with flexible random-deterministic scheme. *The Journal of chemical physics*, 128, 034106 (2008).
- <sup>9</sup> D. Suess, A. Eisfeld, and W. T. Strunz. Hierarchy of stochastic pure states for open quantum system dynamics. *Phys. Rev. Lett* 113, 150403 (2014).
- <sup>10</sup> P. P. Orth, A. Imambekov, and K. Le Hur. Nonperturbative stochastic method for driven spin-boson model. *Phys. Rev. B* 87, 14305 (2013).
- <sup>11</sup> N. Makri and D. E. Makarov. Tensor propagator for iterative quantum time evolution of reduced density matrices. i. theory. *The Journal of Chem. Phys* 102, 4600 (1995).
- <sup>12</sup> L. Diósi, N. Gisin, and W. T. Strunz. Non-markovian quantum state diffusion. *Phys. Rev. A* 58, 1699 (1998).
- <sup>13</sup> J. T. Stockburger and H. Grabert. Non-markovian quantum state diffusion. *Chemical Physics* 268, 249 (2001).
- <sup>14</sup> J. T. Stockburger and H. Grabert. Exact c-number representation of non-markovian quantum dissipation. *Phys. Rev. Lett* 88, 170407 (2002).
- <sup>15</sup> J. T. Stockburger. Simulating spin-boson dynamics with stochastic liouville–von neumann equations. *Chemical Physics* 296, 159 (2004).
- <sup>16</sup> G. M. G. McCaul, C. D. Lorenz, and L. Kantorovich. Partition-free approach to open quantum systems in harmonic environments: An exact stochastic liouville equation. *Phys. Rev. B* 95, 125124 (2017).
- <sup>17</sup> G. M. G. McCaul, C. D. Lorenz, and L. Kantorovich. Driving spin-boson models from equilibrium using exact quantum dynamics. *Phys. Rev. B* 97, 224310 (2018).
- <sup>18</sup> M. A. Lane, D. Matos, I. J. Ford, and L. Kantorovich. Exactly thermalised quantum dynamics of the spin-boson model coupled to a dissipative environment. *arXiv preprint arXiv:2002.07700* (2020).
- <sup>19</sup> H. Grabert, P. Schramm, and G. Ingold. Quantum brownian motion: The functional integral approach. *Physics Reports* 168, 115 (1988).
- <sup>20</sup> H. Imai, Y. Ohtsuki, and H. Kono. Application of stochastic liouville–von neumann equation to electronic energy transfer in fmo complex. *Chemical Physics* 446, 134 (2015).
- <sup>21</sup> K. Schmitz and J. T. Stockburger. A variance reduction technique for the stochastic liouville–von neumann equation. *The European Physical Journal Special Topics* 227, 1929 (2019).
- <sup>22</sup> L. Duan and G. Guo. Reducing decoherence in quantum-computer memory with all quantum bits coupling to the same environment. *Phys. Rev. A* 57, 737 (1998).
- <sup>23</sup> T. A. Costi and R. H. McKenzie. Entanglement between a qubit and the environment in the spin-boson model. *Phys. Rev. A* 68, 34301 (2003).

- <sup>24</sup> C. H. van der Wal, F. K. Wilhelm, C. Harmans, and J. E. Mooij. Engineering decoherence in josephson persistent-current qubits. *The European Physical Journal B - Condensed Matter and Complex Systems* 31, 111 (2003).
- <sup>25</sup> A. Kopp and K. Le Hur. Universal and measurable entanglement entropy in the spin-boson model. *Phys. Rev. Lett* 98, 220401 (2007).
- <sup>26</sup> W. Cui, Z. Xi, and Y. Pan. Non-markovian entanglement dynamics between two coupled qubits in the same environment. *Journal of Physics A: Mathematical and Theoretical* 42, 155303 (2009).
- <sup>27</sup> Y. Makhlin, G. Schön, and A. Shnirman. Quantum-state engineering with josephson-junction devices. *Reviews of Modern Physics* 73, 357 (2001).
- <sup>28</sup> J. Liu, L. Fu, B. Y. Ou, S. G. Chen, D. Choi, B. Wu, and Q. Niu. Theory of nonlinear landau-zener tunneling. *Phys. Rev. A* 66, 23404 (2002).
- <sup>29</sup> D. Valenti, C. Guarcello, and B. Spagnolo. Switching times in long-overlap josephson junctions subject to thermal fluctuations and non-gaussian noise sources. *Phys. Rev. B* 89, 214510 (2014).
- <sup>30</sup> P. P. Orth, D. Roosen, W. Hofstetter, and K. Le Hur. Dynamics, synchronization, and quantum phase transitions of two dissipative spins. *Phys. Rev. B* 82, 144423 (2010).
- <sup>31</sup> P. P. Orth, I. Stanic, and K. Le Hur. Dissipative quantum ising model in a cold-atom spin-boson mixture. *Phys. Rev. A* 77, 51601 (2008).
- <sup>32</sup> D. M. Berns, M. S. Rudner, S. O. Valenzuela, K. K. Berggren, W. D. Oliver, L. S. Levitov, and T. P. Orlando. Amplitude spectroscopy of a solid-state artificial atom. *Nature* 455, 51 (2008).
- <sup>33</sup> S. W. Smith. *The scientist and engineer's guide to digital signal processing*. California Technical Pub. San Diego (1997).
- <sup>34</sup> P. C. Hansen. Deconvolution and regularization with toeplitz matrices. *Numerical Algorithms* 29, 323 (2002).
- <sup>35</sup> A. O. Caldeira and A. J. Leggett. Path integral approach to quantum brownian motion. *Physica A: Statistical mechanics and its Applications* 121, 587 (1983).
- <sup>36</sup> A. V. Oppenheim. *Discrete-Time Signal Processing*. (Upper Saddle River, New Jersey, 1999).
- <sup>37</sup> J. Shao. Rigorous representation and exact simulation of real Gaussian stationary processes. *Chemical Physics* 375, 378 (2010).
- <sup>38</sup> J. L. Starck, E. Pantin, and F. Murtagh. Deconvolution in astronomy: A review. *Publications of the Astronomical Society of the Pacific* 114, 1051 (2002).
- <sup>39</sup> N. Wiener *Extrapolation, interpolation and smoothing of stationary time series with engineering applications* (MIT Press Cambridge, Massachusetts, 1949).
- <sup>40</sup> D. Van de Sompel, L. S. Sasportas, J. V. Jokerst, and S. S. Gambhir. Comparison of deconvolution filters for photoacoustic tomography. *PloS one* 11 (2016).
- <sup>41</sup> C. Zener. Non-adiabatic crossing of energy levels. *Proceedings of the Royal Society of London. Series A, Containing Papers of a Mathematical and Physical Character* 137, 696 (1932).
- <sup>42</sup> C. Wittig. The landau-zener formula. *The Journal of Phys. Chem. B* 109, 8428 (2005).
- <sup>43</sup> A. G. Rojo. Matrix exponential solution of the landau-zener problem. *arXiv preprint arXiv:1004.2914* (2010).
- <sup>44</sup> K. Saito, M. Wubs, S. Kohler, Y. Kayanuma, and P. Hänggi. Dissipative landau-zener transitions of a qubit: Bath-specific and universal behavior. *Phys. Rev. B* 75, 214308 (2007).
- <sup>45</sup> P. Nalbach and M. Thorwart. Landau-zener transitions in a dissipative environment: Numerically exact results. *Phys. Rev. Lett* 103, 220401 (2009).
- <sup>46</sup> M. Wubs, K. Saito, S. Kohler, P. Hänggi, and Y. Kayanuma. Gauging a quantum heat bath with dissipative landau-zener transitions. *Phys. Rev. Lett* 97, 200404 (2006).
- <sup>47</sup> V. B. Braginsky, Y. I. Vorontsov, and K. S. Thorne. Quantum nondemolition measurements. *Science* 209, 547 (1980).
- <sup>48</sup> A. Lupascu, S. Saito, T. Picot, P. C. De Groot, C. J. P. M. Harmans, and J. E. Mooij. Quantum non-demolition measurement of a superconducting two-level system. *Nature Physics* 3, 119 (2007).
- <sup>49</sup> J. Shao, M. Ge, and H. Cheng. Decoherence of quantum-nondemolition systems. *Phys. Rev. E* 53, 1243 (1996).
- <sup>50</sup> H. P. Breuer, E. M. Laine, J. Piilo, and B. Vacchini. Colloquium: Non-Markovian dynamics in open quantum systems. *Reviews of Modern Physics* *Reviews of Modern Physics* 88, 021002 (2016).
- <sup>51</sup> J. S. Tang, C. F. Li, Y. L. Li, X. B. Zou, G. C. Guo, H. P. Breuer, E. M. Laine, and J. Piilo. Measuring non-Markovianity of processes with controllable system-environment interaction. *EPL* 97, 10002 (2012).